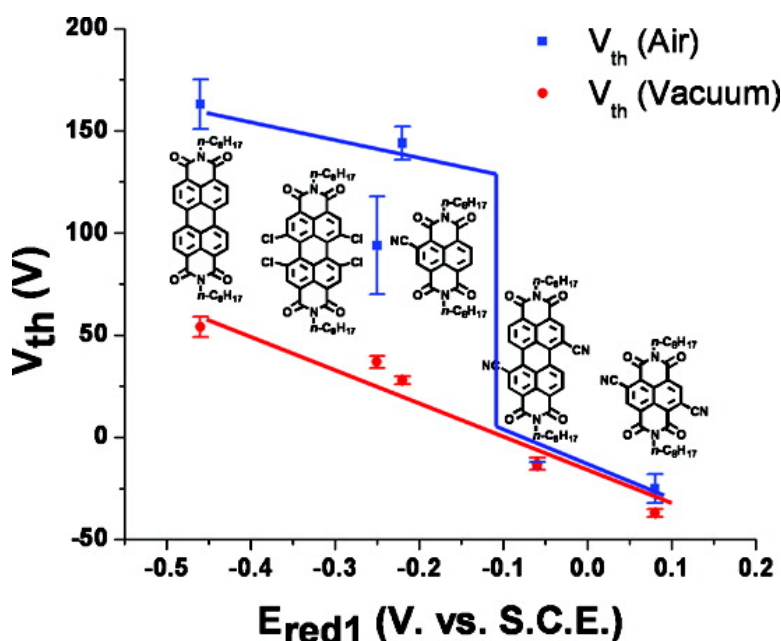## Article

Tuning Orbital Energetics in Arylene Diimide Semiconductors. Materials Design for Ambient Stability of n-Type Charge Transport

Brooks A. Jones, Antonio Facchetti, Michael R. Wasielewski, and Tobin J. Marks

More About This Article

Additional resources and features associated with this article are available within the HTML version:

- Supporting Information
- Access to high resolution figures
- Links to articles and content related to this article
- Copyright permission to reproduce figures and/or text from this article

View the Full Text HTML

Tuning Orbital Energetics in Arylene Diimide Semiconductors. Materials Design for Ambient Stability of n-Type Charge Transport

Brooks A. Jones, Antonio Facchetti, Michael R. Wasielewski,* and Tobin J. Marks*

Contribution from the Department of Chemistry, Materials Research Center, and Argonne-Northwestern Solar Energy Research (ANSER) Center, Northwestern University, Evanston, Illinois 60208-3113

Received July 13, 2007; E-mail: t-marks@northwestern.edu; m-wasielewski@northwestern.edu

Abstract: Structural and electronic criteria for ambient stability in n-type organic materials for organic field-effect transistors (OFETs) are investigated by systematically varying LUMO energetics and molecular substituents of arylene diimide-based materials. Six OFETs on n^+-Si/SiO$_2$ substrates exhibit OFET response parameters as follows: N,N'-bis(n-octyl)perylene-3,4:9,10-bis(dicarboximide) (PDI-8): $\mu = 0.32$ cm^2 V^{-1} s^{-1}, $V_{th} = 55$ V, $I_{on}/I_{off} = 10^5$; N,N'-bis(n-octyl)-1,7- and N,N'-bis(n-octyl)-1,6-dibromoperylene-3,4:9,10-bis-(dicarboximide) (PDI-8Br$_2$): $\mu = 3 \times 10^{-5}$ cm^2 V^{-1} s^{-1}, $V_{th} = 62$ V, $I_{on}/I_{off} = 10^3$; N,N'-bis(n-octyl)-1,6,7,12-tetrachloroperylene-3,4:9,10-bis(dicarboximide) (PDI-8Cl$_4$): $\mu = 4 \times 10^{-3}$ cm^2 V^{-1} s^{-1}, $V_{th} = 37$ V, $I_{on}/I_{off} = 10^4$; N,N'-bis(n-octyl)-2-cyanonaphthalene-1,4,5,8-bis(dicarboximide) (NDI-8CN): $\mu = 4.7 \times 10^{-3}$ cm^2 V^{-1} s^{-1}, $V_{th} = 28$, $I_{on}/I_{off} = 10^5$; N,N'-bis(n-octyl)-1,7- and N,N'-bis(n-octyl)-1,6-dicyanoperylene-3,4:9,10-bis-(dicarboximide) (PDI-8CN$_2$): $\mu = 0.13$ cm^2 V^{-1} s^{-1}, $V_{th} = -14$ V, $I_{on}/I_{off} = 10^3$; and N,N'-bis(n-octyl)-2,6-dicyanonaphthalene-1,4,5,8-bis(dicarboximide) (NDI-8CN$_2$): $\mu = 0.15$ cm^2 V^{-1} s^{-1}, $V_{th} = -37$ V, $I_{on}/I_{off} = 10^2$. Analysis of the molecular geometries and energetics in these materials reveals a correlation between electron mobility and substituent-induced arylene core distortion, while V_{th} and I_{off} are generally affected by LUMO energetics. Our findings also indicate that resistance to ambient charge carrier trapping observed in films of N-(n-octyl)arylene diimides occurs at a molecular reduction potential more positive than ~ -0.1 V (vs SCE). OFET threshold voltage shifts between vacuum and ambient atmosphere operation suggest that, at $E_{red1} < -0.1$ V, the interfacial trap density increases by greater than $\sim 1 \times 10^{13}$ cm^{-2}, while, for semiconductors with $E_{red1} > -0.1$ V, the trap density increase is negligible. OFETs fabricated with the present n-type materials having $E_{red1} > -0.1$ V operate at conventional gate biases with minimal hysteresis in air. This reduction potential corresponds to an overpotential for the reaction of the charge carriers with O$_2$ of ~ 0.6 V. N,N'-1H,1H-Perfluorobutyl derivatives of the perylene-based semiconductors were also synthesized and used to fabricate OFETs, resulting in air-stable devices for all fluorocarbon-substituted materials, despite generally having $E_{red1} < -0.1$ V. This behavior is consistent with a fluorocarbon-based O$_2$ barrier mechanism. OFET cycling measurements in air for dicyanated vs fluorinated materials demonstrate that energetic stabilization of the charge carriers results in greater device longevity in comparison to the OFET degradation observed in air-stable semiconductors with fluorocarbon barriers.

Introduction

The ongoing interest in organic semiconducting materials is driven by the scientific challenges they present as well as by the promise of real-world applications in a multitude of products such as "plastic"/flexible displays, sensors, and RF-ID tags, as recently reviewed.[1−10] The mechanistic, energetic, and structural phenomena governing charge transport in molecular solids have been the subject of an extensive worldwide research effort.[11] Furthermore, recent developments in organic-based light-emitting diodes (OLEDs), photovoltaics (OPVs), and field-effect transistors (OFETs) have opened up many new and exciting challenges and opportunities in the field of thin-film optoelectronics.[12]

One of the major challenges confronting the field of organic electronics has been the development of high-mobility and environmentally stable electron-transporting (n-type) organic semiconductors for thin film device structures to complement the high efficiency/robust nature of current generation p-type materials. The availability of both n- and p-type conductors is

(1) Facchetti, A. *Mater. Today* **2007**, *10*, 28.
(2) Horowitz, G. *Adv. Mater.* **1998**, *10*, 365−377.
(3) Horowitz, G. *J. Mater. Res.* **2004**, *19*, 1946−1962.
(4) Katz, H. E.; Bao, Z. *J. Phys. Chem. B* **2000**, *104*, 671−678.
(5) Würthner, F. *Angew. Chem., Int. Ed.* **2001**, *40*, 1037−1039.
(6) Dimitrakopoulos, C. D.; Malenfant, P. R. L. *Adv. Mater.* **2002**, *14*, 99−117.
(7) Sun, Y.; Liu, Y.; Zhu, D. *J. Mater. Chem.* **2005**, *15*, 53−65.
(8) Chabinyc, M.; Loo, Y.-L. *J. Macromol. Sci., Poly.* **2006**, *46*, 1−5.
(9) Dodabalapur, A. *Nature* **2005**, *434*, 151.
(10) Sirringhaus, H. *Adv. Mater.* **2005**, *17*, 2411.
(11) Pope, M.; Swenberg, C. E. *Electronic Processes in Organic Crystals and Polymers*; 2nd ed.; Oxford University Press: New York, 1999; Vol. 56, p 1328.
(12) Malliaras, G.; Friend, R. *Physics Today* **2005**, *58*, 53−58.

essential for diodes and complementary circuits, structures offering high operating speeds and low power consumption.[13-20] The operational performance and stability of organic n-type materials have significantly lagged behind their p-type counterparts; however in recent years major advances have significantly increased the understanding of n-type charge transport and have suggested strategies for improved materials design.[21-40] One of the major hurdles remaining is the vulnerability of n-type charge carriers to ambient conditions. The capability to design and realize n-type semiconductors where the charge carriers are thermodynamically air-stable would represent an important advance in n-type electronics. Specifically, semiconductors could be tailored to have improved solubility and film-forming properties without concern for risking atmospheric exposure. Given that the ultimate promise of organic semiconductors is in inexpensive, large-area, solution-processed electronics compatible with high throughput reel-to-reel manufacture, the development of air-stable materials is crucial to avoid costly vacuum/inert atmosphere-based fabrication steps and device encapsulation.[41]

The issue of ambient carrier instability in n-type organic semiconductors was first discussed by de Leeuw et al.[42] who analyzed the vulnerability of n-type charge carriers to charge carrier trapping by the most common reactive species in an ambient atmosphere, H_2O and O_2. It is important to note that for most n-type semiconductors, air-instability is not due to intrinsic chemical instability resulting in material decomposition, but rather, air-instability for typical n-type semiconductors is due to the vulnerability of the charge carriers to trapping in ambient conditions, which seriously degrades effective field-effect mobility, and which is frequently reversed upon application of vacuum.[32,43] Consequently, rational strategies for increasing ambient stability must prevent the trapping species from reaching the charge-transporting area of the film and/or to design molecules/polymers in which the mobile electrons are thermodynamically resistant to trapping. It is generally thought that H_2O/O_2 exclusion can be facilitated by utilizing molecular semiconductors which crystallographically pack in a sufficiently dense motif so as to resist film penetration by these species or by appropriately encapsulating the devices in inert atmosphere. Thermodynamic stability is a more complex issue. Based on solution-phase electrochemical potentials, a reduction potential more positive than ~ -0.66 V vs SCE is thought necessary to stabilize the charge carriers in n-type organic materials with respect to H_2O *oxidation*,[42] and materials that satisfy this requirement are known (e.g., C_{60},[44,45] perylene diimides,[46,47] naphthalene diimides,[48-52] and several oligothiophene families[33,53]).[5] However, the thermodynamically founded design of molecular materials with negatively charged carriers not susceptible to *O_2-oxidation*

$$O_2 + 4H^+ = 4e^- \rightleftharpoons 2H_2O$$
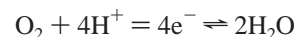
would require a daunting reduction potential greater than $\sim +0.57$ V (vs SCE).[42] While materials with such large electron affinities are rare,[5] an overpotential to the reaction between the charge carriers and O_2 could in principle prevent ambient trapping in materials where the reduction potential was more negative than $\sim +0.57$ V (vs SCE), according to de Leeuw's model.

The most investigated air-stable n-type organic semiconductors include perfluorinated copper phthalocyanine ($CuF_{16}Pc$),[54-60]

(13) Brennan, K. F.; Brown, A. S. *Theory of Modern Electronic Semiconductor Devices*; John Wiley & Sons, Inc.: New York, 2002; p 448.
(14) Jung, T.; Yoo, B.; Wang, L.; Jones, B. A.; Facchetti, A.; Wasielewski, M. R.; Marks, T. J.; Dodabalapur, A. *Appl. Phys. Lett.* **2006**, *88*, 183102.
(15) Yoo, B.; Madgavkar, A.; Jones, B. A.; Nadkarni, S.; Facchetti, A.; Dimmler, D.; Wasielewski, M. R.; Marks, T. J.; Dodabalapur, A. *IEEE Electron Device Lett.* **2006**, *27*, 737−739.
(16) Dodabalapur, A. *Mater. Today* **2006**, *9*, 24−30.
(17) Nadkarni, S.; Yoo, B.; Basu, D.; Dodabalapur, A. *Appl. Phys. Lett.* **2006**, *89*, 184105.
(18) De Vusser, S.; Steudel, S.; Myny, K.; Genoe, J.; Heremans, P. *Appl. Phys. Lett.* **2006**, *88*, 162116.
(19) Hizu, K.; Sekitani, T.; Someya, T.; Otsuki, J. *Appl. Phys. Lett.* **2007**, *90*, 093504.
(20) Klauk, H.; Zschieschang, U.; Pflaum, J.; Halik, M. *Nature* **2007**, *445*, 745−748.
(21) Newman, C. R.; Frisbie, C. D.; da Silva Filho, D. A.; Brédas, J.-L.; Ewbank, P. C.; Mann, K. R. *Chem. Mater.* **2004**, *16*, 4436−4451.
(22) Facchetti, A.; Deng, Y.; Wang, A.; Koide, Y.; Sirringhaus, H.; Marks, T. J.; Friend, R. H. *Angew. Chem.* **2000**, *39*, 4547−4551.
(23) Facchetti, A.; Hutchison, G.; Yoon, M.-H.; Letizia, J.; Ratner, M. A.; Marks, T. J. *Polym. Prepr. (Am. Chem. Soc., Div. Polym. Chem.)* **2004**, *45*, 185.
(24) Facchetti, A.; Letizia, J.; Yoon, M.-H.; Mushrush, M.; Katz, H. E.; Marks, T. J. *Chem. Mater.* **2004**, *16*, 4715−4724.
(25) Facchetti, A.; Mushrush, M.; Katz, H. E.; Marks, T. J. *Angew. Chem., Int. Ed.* **2003**, *15*, 33−38.
(26) Facchetti, A.; Mushrush, M.; Yoon, M.-H.; Hutchison, G. R.; Ratner, M. A.; Marks, T. J. *J. Am. Chem. Soc.* **2004**, *126*, 13859−13874.
(27) Facchetti, A.; Yoon, M.-H.; Stern, C. L.; Hutchison, G. R.; Ratner, M. A.; Marks, T. J. *J. Am. Chem. Soc.* **2004**, *126*, 13480−13501.
(28) Facchetti, A.; Yoon, M.-H.; Stern, C. L.; Katz, H. E.; Marks, T. J. *Angew. Chem.* **2003**, *42*, 3900−3903.
(29) Hutchison, G. R.; Ratner, M. A.; Marks, T. J. *J. Am. Chem. Soc.* **2005**, *127*, 16866−16881.
(30) Hutchison, G. R.; Ratner, M. A.; Marks, T. J. *J. Am. Chem. Soc.* **2005**, *127*, 2339−2350.
(31) Jones, B. A.; Ahrens, M. J.; Yoon, M.-H.; Facchetti, A.; Marks, T. J.; Wasielewski, M. R. *Angew. Chem., Int. Ed.* **2004**, *43*, 6363−6366.
(32) Letizia, J. A.; Facchetti, A.; Stern, C. L.; Ratner, M. A.; Marks, T. J. *J. Am. Chem. Soc.* **2005**, *127*, 13476−13477.
(33) Yoon, M.-H.; DiBenedetto, S.; Facchetti, A.; Marks, T. J. *J. Am. Chem. Soc.* **2005**, *127*, 1348−1349.
(34) Cai, X.; Burand, M. W.; Newman, C. R.; da Sliva Filho, D. A.; Pappenfus, T. M.; Bader, M. M.; Bredas, J.-L.; Mann, K. R.; Frisbie, C. D. *J. Phys. Chem. B* **2006**, *110*, 14590−14597.
(35) Cavallini, M.; Stoliar, P.; Moulin, J.-F.; Surin, M.; Leclere, P.; Lazzaroni, R.; Breiby, D. W.; Andreasen, J. W.; Nielsen, M. M.; Sonar, P.; Grimsdale, A. C.; Muellen, K.; Biscarini, F. *Nano Lett.* **2005**, *5*, 2422−2425.
(36) Coropceanu, V.; Cornil, J.; Da Silva Filho, D. A.; Olivier, Y.; Silbey, R.; Brédas, J.-L. *Chem. Rev.* **2007**, *107*, 2165.
(37) Nolde, F.; Pisula, W.; Mueller, S.; Kohl, C.; Müellen, K. *Chem. Mater.* **2006**, *18*, 3715−3725.
(38) Pisula, W.; Menon, A.; Stepputat, M.; Lieberwirth, I.; Kolb, U.; Tracz, A.; Sirringhaus, H.; Pakula, T.; Müellen, K. *Adv. Mater.* **2005**, *17*, 684−489.
(39) Wu, J.; Wojciech, P.; Müellen, K. *Chem. Rev.* **2007**, *107*, 718−747.
(40) Zhang, M.; Tsao, H. N.; Pisula, W.; Yang, C.; Mishra, A. K.; Müellen, K. *J. Am. Chem. Soc.* **2007**, *129*, 3472−3473.
(41) Bao, Z. *Adv. Mater.* **2000**, *12*, 227−230.

(42) de Leeuw, D. M.; Simenon, M. M. J.; Brown, A. R.; Einerhand, R. E. F. *Synth. Met.* **1997**, *87*, 53−59.
(43) Chesterfield, R. J.; McKeen, J. C.; Newman, C. R.; Ewbank, P. C.; da Silva Filho, D. A.; Brédas, J.-L.; Miller, L. L.; Mann, K. R.; Frisbie, C. D. *J. Phys. Chem. B* **2004**.
(44) Kalbac, M.; Kavan, L.; Zukalova, M.; Dunsch, L. *J. Am. Chem. Soc.* **2006**.
(45) Jousselme, B.; Sonmez, G.; Wudl, F. *J. Mater. Chem.* **2006**, *16*, 3478−3482.
(46) Gosztola, D.; Niemczyk, M. P.; Svec, W. *J. Phys. Chem. A* **2000**, *104*, 6545−6551.
(47) van der Boom, T.; Hayes, R. T.; Zhao, Y.; Bushard, P. J.; Weiss, E. A.; Wasielewski, M. R. *J. Am. Chem. Soc.* **2002**, *124*, 9582−9590.
(48) Katz, H. E.; Johnson, J.; Lovinger, A. J.; Wenjie, L. *J. Am. Chem. Soc.* **2000**, *122*, 7787−7792.
(49) Lukas, A. S.; Bushard, P. J.; Wasielewski, M. R. *J. Phys. Chem. A* **2002**, *106*, 2074−2082.
(50) Miller, S. E.; Lukas, A. S.; Marsh, E.; Bushard, P.; Wasielewski, M. R. *J. Am. Chem. Soc.* **2000**, *122*, 7802−2810.
(51) Miller, S. E.; Zhao, Y.; Schaller, R.; Mulloni, V.; Just, E. M.; Johnson, R. C.; Wasielewski, M. R. *Chem. Phys.* **2002**, *275*, 167−183.
(52) Wiederrecht, G. P.; Svec, W. A.; Wasielewski, M. R.; Galili, T.; Levanon, H. *J. Am. Chem. Soc.* **2000**, *122*, 9715−9722.
(53) Chesterfield, R. J.; Newman, C. R.; Pappenfus, T. M.; Ewbank, P. C.; Haukaas, M. H.; Mann, K. R.; Miller, L. L.; Frisbie, C. D. *Adv. Mater.* **2003**, *15*, 1278−1282.
(54) Bao, Z.; Lovinger, A. J.; Brown, J. *J. Am. Chem. Soc.* **1998**, *120*, 207−208.

Chart 1. Structures of Some Known Air-Stable n-Type Organic Semiconductors, Their Reduction Potentials, and Reported FET Mobilities: $CuF_{16}Pc$, NDI-F, NDI-XF, PDI-FCN$_2$, PDI-CN$_2$, and NDI-8CN$_2$
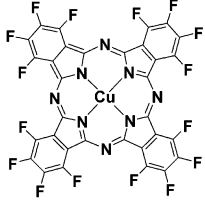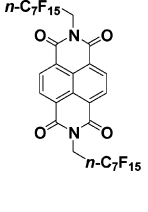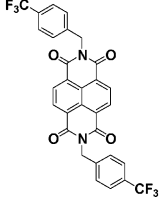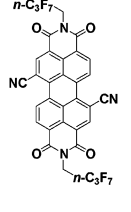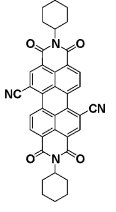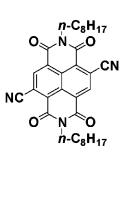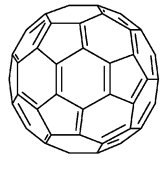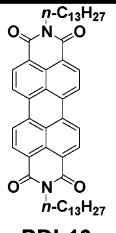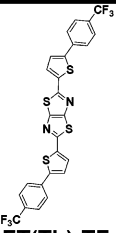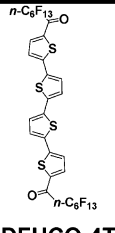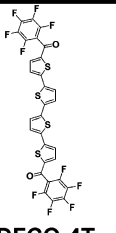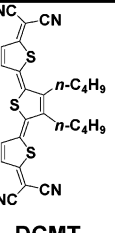
	$CuF_{16}Pc$	NDI-F	NDI-XF	PDI-FCN$_2$	PDI-CN$_2$	NDI-8CN$_2$
E_{red1} (S.C.E.)	-0.13	-0.4 V	-0.5 V	+0.03 V	-0.07 V	+0.08 V
$\mu(cm^2V^{-1}s^{-1})$	0.03	0.05	0.1	0.6	0.1	0.15

Chart 2. Structures of Some High Mobility Air-Unstable n-Type Organic Semiconductors, Their Reduction Potentials, and Reported FET Mobilities: C$_{60}$, PDI-13, FT(Th)$_2$TF, DFHCO-4T, and DFCO-4T

	C$_{60}$	PDI-13	FT(Th)$_2$TF	DFHCO-4T	DFCO-4T	DCMT
E_{red1} (S.C.E.)	-0.5 V	-0.46 V	-1.54 V	-0.88 V	-1.05 V	-0.19
$\mu(cm^2V^{-1}s^{-1})$	0.5	2.1	1.2	1.7	0.5	0.2

fluoroacyl oligothiophenes (DFCO-4TCO),[33] *N,N′*-fluorocarbon-substituted naphthalene diimides (NDI-F, NDI-XF),[61−63] cyano-substituted perylene diimides (PDI-CN$_2$, PDI-FCN$_2$),[14,15,31,64,65] and cyano-substituted naphthalene diimides (NDI-8CN$_2$)[66] (Chart 1). With the exception of the NDI and PDI derivatives which are imide-substituted oligo-naphthalenes, collectively known as arylene diimides or rylene diimides for the larger homologues,[67] the electrical performance of TFT devices fabricated with these air-stable materials does not approach that

of high mobility but of air-sensitive materials such as C$_{60}$,[68−70] PDI-8,[43,71] PDI-13,[72] FT(Th)$_2$TF,[73,74] DFHCO-4T,[33,58] DFCO-4T,[32] and DCMT[53,75] (Chart 2).[76]

For these reasons, members of the arylene imide family are a particularly attractive class of target materials to explore because of their robust nature, flexible molecular orbital energetics, and excellent charge transport properties that should be tailorable via judicious functionalization. Interestingly, the onset of ambient stability in these semiconductors could in principle be achieved via two different design strategies: (i) introduction of fluorinated substituents (R^F) at the *N,N′* positions to create close-packed solid-state atmospheric barriers[48,54,62,63,77]

(55) de Oteyza, D. G.; Barrena, E.; Osso, J. O.; Dosch, H.; Meyer, S.; Pflaum, J. *Appl. Phys. Lett.* **2005**, *87*, 183504.
(56) Schön, J. H.; Kloc, C.; Bao, Z.; Batlogg, B. *Adv. Mater.* **2000**, *12*, 1539−1542.
(57) Ye, R.; Baba, M.; Oishi, Y.; Mori, K.; Suzuki, K. *Appl. Phys. Lett.* **2005**, *86*, 253505.
(58) Yoon, M.-H.; Kim, C.; Facchetti, A.; Marks, T. J. *J. Am. Chem. Soc.* **2006**, *128*, 12851−12869.
(59) Tong, W. Y.; Djurišić, A. B.; Xie, M. H.; Ng, A. C. M.; Cheung, K. Y.; Chan, W. K.; Leung, Y. H.; Lin, H. W.; Gwo, S. *J. Phys. Chem. B* **2006**, *110*, 17406−17413.
(60) Yuan, J.; Zhang, J.; Wang, J.; Yan, D.; Xu, W. *Thin Solid Films* **2004**, *450*, 316−319.
(61) Katz, H. E.; Johnson, J.; Lovinger, A. J.; Li, W. *J. Am. Chem. Soc.* **2000**, *122*, 7787−7792.
(62) Katz, H. E.; Lovinger, A. J.; Johnson, J.; Kloc, C.; Seigrist, T.; Li, W.; Lin, Y.-Y.; Dodabalapur, A. *Nature* **2000**, *404*, 478−481.
(63) Katz, H. E.; Siegrist, T.; Schön, J. H.; Kloc, C.; Batlogg, B.; Lovinger, A. J.; Johnson, J. *ChemPhysChem* **2001**, *3*, 167−172.
(64) Ahrens, M. J.; Fuller, M. J.; Wasielewski, M. R. *Chem. Mater.* **2003**, *15*, 2684−2686.
(65) Yoo, B.; Jung, T.; Basu, D.; Dodabalapur, A.; Jones, B. A.; Facchetti, A.; Wasielewski, M. R.; Marks, T. J. *Appl. Phys. Lett.* **2006**, *88*, 082104.
(66) Jones, B. A.; Facchetti, A.; Marks, T. J.; Wasielewski, M. R. *J. Am. Chem. Soc.* **2006**.
(67) Herrmann, A.; Müllen, K. *Chem. Lett.* **2006**, *35*, 978−985.

(68) Haddon, R. C.; Perel, A. S.; Morris, R. C.; Palstra, T. T. M.; Hebard, A. F.; Fleming, R. M. *Appl. Phys. Lett.* **1995**, *67*, 121−123.
(69) Kobayashi, S.; Nishikawa, T.; Takenobu, T.; Mori, S.; Shimoda, T.; Mitani, T.; Shimotani, H.; Yoshimoto, N.; Ogawa, S.; Iwasa, Y. *Nat. Mater.* **2004**, *3*, 317−322.
(70) Bossard, C.; Rigaut, S.; Astruc, D.; Delville, M. H.; Félix, G.; Février-Bouvier, A.; Amiell, J.; Flandrois, S.; Delhaès, P. *J. Chem. Soc., Chem. Commun.* **1993**, 333−334.
(71) Malenfant, P. R. L.; Dimitrakopoulos, C. D.; Gelorme, J. D.; Kosbar, L. L.; Graham, T. O.; Curioni, A.; Andreoni, W. *Appl. Phys. Lett.* **2002**, *80*, 2517−2519.
(72) Tatemichi, S.; Ichikawa, M.; Koyama, T.; Taniguchi, Y. *Appl. Phys. Lett.* **2006**, *89*, 112108.
(73) Ando, S.; Nishida, J.-i.; Tada, H.; Inoue, Y.; Tokito, S.; Yamashita, Y. *J. Am. Chem. Soc.* **2005**, *127*, 5336−5337.
(74) Kumaki, D.; Ando, S.; Shimono, S.; Yamashita, Y.; Umeda, T.; Tokito, S. *Appl. Phys. Lett.* **2007**, *90*, 053506.
(75) Pappenfus, T. M.; Chesterfield, R. J.; Frisbie, C. D.; Mann, K. R.; Casado, J.; Raff, J. D.; Miller, L. L. *J. Am. Chem. Soc.* **2002**, *124*, 4184−4185.
(76) Letizia, J. A.; Facchetti, A.; Stern, C. L.; Ratner, M. A.; Marks, T. A. J. *Am. Chem. Soc.* **2005**, *127*, 13476−13477.

or (ii) addition of highly electron-withdrawing core substituents, thereby lowering the energies of the LUMO/charge carriers below that of most atmospheric trapping species.[21,42,78]

In the case of NDI-F or asymmetric derivatives with a single R^F chain, the addition of fluorocarbon substituents to the *N,N'* positions does not significantly lower the molecular reduction potentials relative to the fluorine-free analogues; however, OFETs fabricated with films of the fluorinated materials are reported to exhibit air-stable device operation while the fluorine-free analogues do not.[48,77] Since the R^F chains do not significantly alter the LUMO energies of these NDI derivatives ($\Delta E \leq 0.15$ eV), a steric barrier to atmospheric penetration created by the densely packed R^F groups is thought to be responsible for the charge carrier air stability.[6,48,62] Furthermore, in the case of NDI-XF, the reduction potential is also nearly identical to that of the non-fluorinated derivative.[48] In this case as well, only the fluorinated materials exhibit ambient OFET stability. Recently, PDI-based materials with fluoro-substituted phenyl groups at the *N,N'* positions were shown to yield air-stable OFET operation despite having similar reduction potentials to the non-fluorinated parent.[79,80] Interestingly, the air stability was also shown to be dependent on the fluorination level and fluorine substitution pattern.[79] To explain this general behavior, Katz et al. proposed that the larger fluorine van der Waals radius relative to hydrogen leads to a decreased available spacing between the *N,N'*-chains from ~4 Å to ~2 Å, thus preventing O_2 intrusion[62] (Figure 1).

In the case of $CuF_{16}Pc$, the air-stable device behavior is thought to reflect a combination of a close-packing O_2 barrier and the low-lying LUMO of the material.[54] The analogous chlorinated material, $CuCl_{16}Pc$, is also reported to support air-stable OFET operation because of the low-energy charge carriers.[81] Non-fluorinated air-stable organometallic- and fullerene-based semiconductors with LUMO energies more negative than ~ −4.0 eV also show resistance to air-derived electron traps.[82] Recently, we reported ambient operational stability and high carrier mobilities in the cyanated perylene diimides, PDI-CN$_2$ and PDI-FCN$_2$,[31] and the cyanated naphthalene diimide, NDI-8CN$_2$.[83] While PDI-FCN$_2$ has fluorinated functionalities that can provide a barrier analogous to the aforementioned air-stable materials, the *N*-hydroalkyl functionalized structures of PDI-CN$_2$ and NDI-8CN$_2$ are unique among air-stable n-type organic semiconductors because the *N*-alkyl groups (R^H) cannot provide the same kind of barrier to atmospheric electron traps as the *N*-R^F chains.

In addition to these results, work from other groups has documented the air instability of *N*-alkyl PDI and NDI derivatives. Thus, Malenfant et al. demonstrated that OFETs fabricated with *N,N'*-n-octyl PDI derivatives possess excellent electrical properties but that the performance degrades rapidly in air.[71] Furthermore, the same behavior is observed in *N,N'*-n-octyl NDI
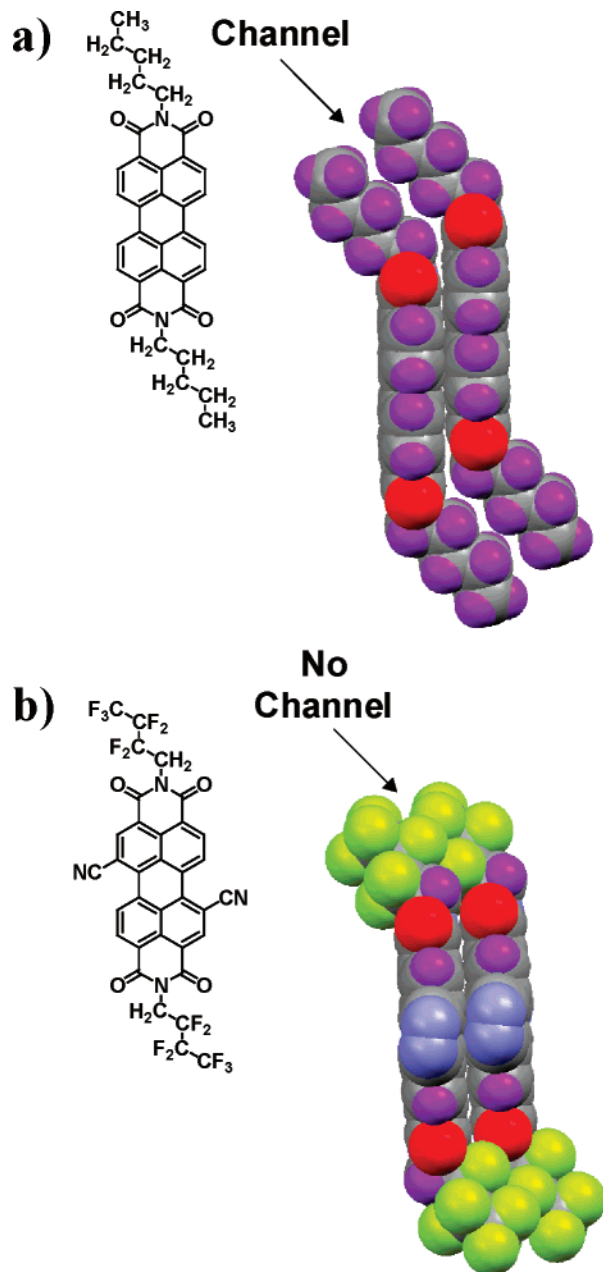

Figure 1. Space-filling models of PDI-based dimers taken from the published crystal structures. The model of air-unstable *N,N'*-n-pentyl-PDI (a) depicts the channels between hydrogen atoms (purple) of adjacent hydrocarbon *N,N'*-groups that is postulated to facilitate ambient-derived charge carrier trap penetration into the film. The model of air-stable PDI-FCN$_2$ (b) depicts the substantial contraction of the channels between the fluoroalkyl chains (green), relative to the hydrocarbon case in (a) that has been proposed to present a barrier to penetration of ambient-derived charge carrier traps in fluorinated phthalocyanines as well as in naphthalene and perylene diimides.

derivatives.[48,62] More recently, Bao et al. reported that *N,N'*-cyclohexyl PDI devices also fail in air.[84] Frisbie et al. shed light on the mechanism of such device failures by increasing the O_2 partial pressure in the operating atmosphere for OTFT devices fabricated with *N,N'*-n-pentyl PDI derivatives and reported a positive shift in threshold voltage with increasing O_2 partial pressure during operation. This shift can be assigned to the

(77) Katz, H. E.; Otsuki, J.; Yamazaki, K.; Suka, A.; Takido, T.; Lovinger, A. J.; Raghavachari, K. *Chem. Lett.* **2003**, *32*, 508−509.
(78) Laquindanum, J. G.; Katz, H. E.; Dodabalapur, A.; Lovinger, A. J. *J. Am. Chem. Soc.* **1996**, *118*, 11331−11332.
(79) Chen, H. A.; Ling, M. M.; Mo, X.; Shi, M. M.; Wang, M.; Bao, Z. *Chem. Mater.* **2007**, *19*, 816−824.
(80) Hosoi, Y.; Tsunami, D.; Ishii, H.; Furukawa, Y. *Chem. Phys. Lett.* **2007**, *436*, 139−143.
(81) Ling, M.-M.; Bao, Z. *Appl. Phys. Lett.* **2006**, *89*, 163516.
(82) Anthopoulos, T. D.; Anyfantis, G. C.; Papavassiliou, G. C.; de Leeuw, D. M. *Appl. Phys. Lett.* **2007**, *90*, 122105.
(83) Jones, B. A.; Facchetti, A.; Marks, T. J.; Wasielewski, M. R. *Chem. Mater.* **2007**, *19*, 2703−2705.
(84) Locklin, J.; Li, D.; Mannsfeld, S. C. B.; Borkert, E.-J.; Meng, H.; Advincula, R.; Bao, Z. *Chem. Mater.* **2005**, *17*, 3366−3374.

creation of metastable PDI/O_2 trap states.[85] Given that O_2-derived trap formation in arylene diimide semiconductor films is found to occur when the *N*,*N′* substituents are either saturated or aromatic hydrocarbon functionalities, it would appear that the mechanism for air stability in the analogous cyano-substituted materials (PDI-CN_2 and NDI-$8CN_2$) is markedly different from that invoked in the case of the aforementioned *N*-fluorocarbon materials.

In this contribution, we investigate the effects on OFET performance, in both vacuum and ambient, of increasing molecular electron affinity in a series of arylene diimide semiconductors. The energetics, thin film morphology and microstructure, and crystal packing in a homologous series of similar derivatives are systematically analyzed to understand the differences in transistor performance for the series, and from these data a value for the overpotential to ambient charge carrier oxidation in this family of n-type semiconductors can be estimated.

Experimental Section

The synthesis and purification of all arylene diimide materials were accomplished using slight modifications of literature procedures; see Supporting Information for further details.[86–88] ^{1}H NMR spectra (400 MHz) were measured in CDCl$_3$ on a Varian Mercury 400 instrument, with chemical shifts referenced to the internal CHCl$_3$ resonance. The 600 MHz ^{1}H NMR spectrum of PDI-$8Br_2$ in CHCl$_3$ was acquired on a Varian INOVA 600 instrument to obtain the dibromo 1,6-/1,7- PDI substitutional isomer ratio. Optical absorption spectra were acquired on a Shimadzu 1601 spectrophotometer. Emission spectra were acquired on a PTI single photon counting spectrofluorimeter in a right angle configuration. Cyclic voltammetry was conducted under N_2 in dry 0.1 M TBAPF$_6$ in dichloromethane solutions and was referenced to Fc/Fc$^+$ (0.475 vs SCE).

Films of the semiconductors were grown from the vapor phase (2 × 10^{-6} Torr, 0.2 Å/s, ∼50 nm thick) on n$^+$-Si (001) wafers having 300 nm of thermally grown SiO$_2$ as the dielectric layer (Montco Silicon Tech). The wafers were cleaned by rinsing with acetone, methanol, and isopropanol followed by a 5 min plasma cleaning in a Harrick Plasma Cleaner/Sterilizer PDC-32G. Substrates for PDI–FBr$_2$ and PDI–FCl$_4$ thin film deposition were exposed to hexamethyldisilzane (HMDS) vapor for 3 days prior to semiconductor film deposition, because films grown on SiO$_2$ did not yield active OFETs.

Tapping-mode AFM images were obtained on a Digital Instruments Multimode Nanoscope IIIa instrument with Nanoprobe TESP-70 tips (cantilever length = 125 μm, freq = 278–338 kHz). X-ray diffraction (Θ/2Θ and ω scans) was performed on a Rigaku ATXG thin film diffractometer in slit-configuration with a Ni-filtered Cu source. Reduced pressure TGA/DTA data were obtained on a TA Instruments SDT 2960 unit interfaced with a mechanical vacuum pump.

Top-contact TFTs were fabricated by vapor depositing Au (3 × 10^{-6} Torr, 0.3 Å/s, ∼50 nm thick) onto the semiconductor thin films through a shadow mask to obtain devices with a channel width of 100 μm and length of 5 mm. Electrical measurements were performed with a Keithley 6430 subfemtoammeter and a Keithley 2400 source meter in ambient atmosphere or in a vacuum probe station at 10^{-6} Torr, as described previously.[32] Care was taken to protect the OFETs from ambient light prior to and during electrical measurements. The durability of PDI-$8CN_2$, PDI-F, and PDI-FCN_2 TFTs operating under ambient

conditions was investigated by cycling the devices immediately after breaking vacuum at V_d = +100 V between a V_g slightly more positive than the "off" state and a V_g in the "on" state for 1000 cycles using a gate delay of 0.1 s. Transfer plots were taken before (cycle 0) and after (cycle 1001) to compare electrical parameters before and after. The entire cycling measurement takes approximately 1 h and 30 min. The "on" V_g and "off" V_g are (+100 V/−25 V) for PDI-$8CN_2$, (+100 V/+25 V) for PDI-F, and (+75 V/−25 V) for PDI-FCN_2.

Electronic structure calculations were performed in SpartanPC.[89,90] Initial geometry optimizations were performed using semiempirical PM3 methods. The resulting geometry was used as a starting point for geometry optimization and frontier molecular orbital energy calculations using DFT/B3LYP with a 6-31G* basis set.

Results

In the following sections we first discuss the synthesis and characterization of the semiconductors used in this study, including modifications to the previously reported synthetic methodologies, and present an analysis of the regioisomer distributions associated with disubstituted PDIs. We then present reduced pressure thermogravimetric/differential thermal analysis characterization of the volatility and phase transitions, followed by electronic structure characterization via electrochemistry, optical spectroscopy, and DFT computations. Finally, the microstructures and transport properties of thin films are compared using X-ray diffraction, tapping-mode atomic force microscopy, and OFET measurements. The OFET measurements are performed both under high vacuum and in ambient atmosphere.

Synthesis. A series of 10 arylene diimide semiconductors was synthesized for this study (Chart 3). Details of the NDI-8CN, NDI-$8CN_2$, PDI-FBr_2, and PDI-FCN_2 syntheses have already been reported.[31,66] The synthesis and purification of semiconductors PDI-8, PDI-$8Br_2$, and PDI-$8Cl_4$ were carried out with modifications of previously reported procedures.[86–88] PDI-8 and PDI-F were synthesized by condensation of perylene dianhydride (PDA) with *n*-octylamine or 1*H*,1*H*-perfluorobu-tylamine, respectively, in molten imidazole;[86] however, the reaction was performed in a sealed tube to achieve a reasonable yield of PDI-F, presumably due to the volatility of the fluorinated amine. PDI-$8Br_2$, PDI-FCl_4, and PDI-$8Cl_4$ were prepared by refluxing a mixture of the halogenated dianhydride and the corresponding amine, *n*-octyl amine or 1*H*,1*H*-perfluo-robutylamine, in propionic acid to prevent amine substitution at the halogenated positions.[87] All semiconductors were purified by multiple gradient vacuum sublimations, with the exception of PDI-$8Br_2$, PDI-$8Cl_4$, and PDI-$8CN_2$ to avoid thermal decomposition during sublimation. These three materials were purified by chromatography on silica followed by multiple recrystallizations.

The current, improved PDI-$8CN_2$ synthesis involves significant modifications to the previously reported procedure (see Supporting Information for details).[31,64] The bromination and imide condensation were accomplished via known methodologies; however, cyanation was achieved by heating a DMF solution of the dibromo-PDI to 130 °C with a 10-fold excess of CuCN. Previously, we reported that CuCN did not achieve efficient cyanation of the PDI-core;[64] however with the new methodology recently utilized for NDI-$8CN_2$ synthesis,[66] we

(85) Chesterfield, R. J.; McKeen, J. C.; Newman, C. R.; Frisbie, C. D. *J. Appl. Phys.* **2004**, *95*, 6396–6405.
(86) Demmig, S.; Langhals, H. *Chem. Ber.* **1988**, *121*, 225–230.
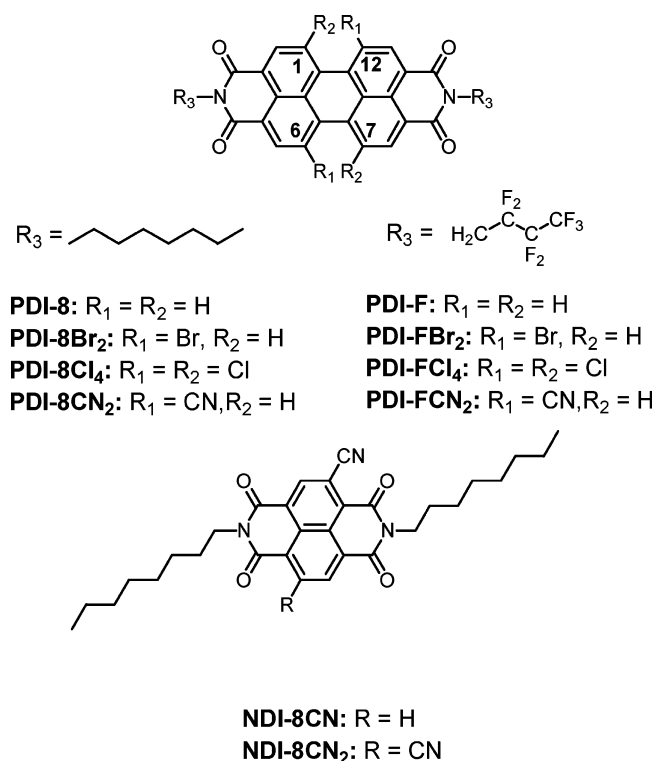(87) Chen, Z.; Debije, M. G.; Debaerdemaeker, T.; Osswald, P.; Würthner, F. *ChemPhysChem* **2004**, *5*, 137–140.
(88) Würthner, F.; Stepanenko, V.; Chen, Z.; Saha-Moller, C. R.; Kocher, N.; Stalke, D. *J. Org. Chem.* **2004**, *69*, 7933–7939.

(89) *Spartan '06*; Wavefunction, Inc.: Irvine, CA.
(90) Shao, Y. et al. *Phys. Chem. Chem. Phys.* **2006**, *8*, 3172–3191.

Chart 3. Chemical Structures of the *N,N′-n*-Octyl and *N,N′*-1*H*,1*H*-Perfluorobutyl Perylene Diimide Semiconductors and *N,N′-n*-Octyl Naphthalene Diimide Semiconductors Investigated in This Study

PDI-8: $R_1 = R_2 = H$
PDI-8Br$_2$: $R_1 = Br, R_2 = H$
PDI-8Cl$_4$: $R_1 = R_2 = Cl$
PDI-8CN$_2$: $R_1 = CN, R_2 = H$

PDI-F: $R_1 = R_2 = H$
PDI-FBr$_2$: $R_1 = Br, R_2 = H$
PDI-FCl$_4$: $R_1 = R_2 = Cl$
PDI-FCN$_2$: $R_1 = CN, R_2 = H$

NDI-8CN: R = H
NDI-8CN$_2$: R = CN

realize efficient cyanation with CuCN instead of the Pd-catalyzed methodology.[31,64]

As reported previously,[31] the synthesis of significant quantities of isomerically pure disubstituted PDIs remains problematic, a consequence of perylene dianhydride bromination leading to a mixture of 1,6 and 1,7 isomers.[31,88] Separating the 1,6 and 1,7 isomers of PDI-8Br$_2$ and PDI-8CN$_2$ presents a challenge, and repeated fractional recrystallizations[88] involving the slow diffusion of MeOH into methylene chloride solutions of PDI-8Br$_2$ isomeric mixtures yields products enriched to ∼65% (by ^{1}H NMR) in the 1,7 isomer and analogous procedures yield ∼73% enrichment (by ^{1}H NMR) in the 1,7-isomer for PDI-8CN$_2$. Attempts to separate the two isomers by either normal or reversed-phase HPLC did not yield acceptable separations. The effects on OFET performance of having multiple regioisomers present in these samples are unclear because the synthesis of sufficient quantities of regioisomerically pure materials for thin film depositions has proven difficult. However, we have reported the crystal structure of a PDI-FCN$_2$ sample in which both regioisomers cocrystallize,[31] suggesting that in the dicyanated case the presence of two isomers does not significantly affect crystal packing. Also note that the 1*H*,1*H*-perfluorobutyl substituted semiconductors were also synthesized and characterized to compare reduction potentials and air-stable OFET operation versus the *n*-octyl materials. Consequently, the 1*H*,1*H*-perfluorobutyl materials and their thin films were not exhaustively optimized and characterized.

Thermal Characterization. Reduced pressure (10.0 Torr under N$_2$, 2 °C/min temperature ramp) simultaneous thermogravimetric analysis-differential thermal analysis (TGA-DTA) scans were performed to evaluate the volatility and thermal

stability of PDI-8, PDI-8Br$_2$, PDI-8Cl$_4$, and PDI-8CN$_2$ (Figure S2). The degree of source material decomposition products in a vapor-phase deposition can have significant effects on impurity levels in the resulting thin films. Chemical contaminants can contribute to unintentional doping, thereby increasing off-currents, depressing on−off current ratios (I_{on}/I_{off}), and/or creating carrier traps which reduce mobility.[91] At this relatively low-pressure level, PDI-8, PDI-8Cl$_4$, and PDI-8CN$_2$ exhibit minimal decomposition, as indicated by nonvolatile residues of ∼1, ∼6, and ∼8 wt %, respectively. PDI-8Br$_2$ undergoes substantial decomposition at 10 Torr with ∼20 wt % nonvolatile residue, meaning that impurities/traps from decomposed material created during film deposition likely compromise device performance. To minimize impurities from decomposition of the source material, fresh semiconductor samples were used for every film growth experiment to minimize film contamination by dehalogenated or decyanated species.

In addition to information about decomposition, the melting points from the DTA scans provide insight into the relative cohesive energetics of the intermolecular interactions in the solid state. In general, strong intermolecular interactions in molecular solids correlate with greater intermolecular orbital overlap, resulting in greater carrier mobilities.[4] The DTA reveals melting points of 200, 233, and 300 °C for PDI-8Br$_2$, PDI-8Cl$_4$, and PDI-8CN$_2$, respectively. Moreover, the DTA data for PDI-8 exhibit two transitions at 220 and 375 °C, where the first transition is in good agreement with the previously reported liquid crystalline (LC) phase transition for this derivative.[92] The increased ordering in LC phases of *N*-alkyl PDI semiconductors has been previously invoked to explain the exceptionally large electron mobilities in these materials.[92,93] While LC phases of core-substituted PDIs have been reported, these molecules do not have *N*-alkyl functionalization.[94−96]

Electronic Structure Characterization. The electronic properties of all the present semiconductors were characterized by cyclic voltammetry (CV), UV−visible optical absorption spectroscopy (UV−vis), and photoluminescence spectroscopy (PL). DFT level electronic structure calculations were performed for each core to probe orbital energetics and the most stable geometry. The relative HOMO and LUMO energetic positions are crucial in determining the majority charge carrier[26,29,30] and charge carrier stability in typical organic semiconductors.[25] In the case of organic n-type materials where charge transport occurs predominantly by hopping through low-lying LUMOs, energies < −3 eV vs vacuum are generally thought necessary for efficient electron injection into the semiconductor.[21,26,29,30] Additionally, the lower the LUMO energy, the lower the bias required to inject carriers should be and the less susceptible the electrons should be to trapping. The LUMO energies for the semiconductors in this study were estimated by conventional

(91) Katz, H. E.; Bao, Z.; Gilat, S. L. *Acc. Chem. Res.* **2001**, *34*, 359−369.
(92) Struijk, C. W.; Sieval, A. B.; Dakhorst, J. E. J.; van Dijk, M.; Kimkes, P.; Koehorst, R. B. M.; Donker, H.; Schaafsma, T. J.; Picken, S. J.; van de Craats, A. M.; Warman, J. M.; Zuilhof, H.; Sudhölter, E. J. R. *J. Am. Chem. Soc.* **2000**, *122*, 11057−11066.
(93) An, Z.; Yu, J.; Jones, S. C.; Barlow, S.; Yoo, S.; Domercq, B.; Prins, P.; Siebbeles, L. D. A.; Kippelen, B.; Marder, S. R. *Adv. Mater.* **2005**, *17*, 2580−2583.
(94) Fuller, M. J.; Sinks, L. E.; Rybtchinski, B.; Giaimo, J. M.; Xiyou, L.; Wasielewski, M. R. *J. Phys. Chem. A* **2005**, *109*, 970−975.
(95) Fuller, M. J.; Walsh, C. J.; Zhao, Y.; Wasielewski, M. R. *Chem. Mater.* **2002**, *14*, 952−953.
(96) Fuller, M. J.; Wasielewski, M. R. *J. Phys. Chem. B* **2001**, *105*, 7216−7219.

Table 1. Frontier Molecular Orbital Energies of the Organic Semiconductors Studied in This Contribution Estimated from Cyclic Voltammetry[a,b] and Optical Absorption/Emission[c] Measurements

semiconductor	$E_{red1}{}^a$	LUMO[b] (eV)	HOMO[c] (eV)	$\lambda_{abs}{}^d$ (nm)	$\lambda_{em}{}^d$ (nm)	$E_g{}^d$ (eV)
PDI-8	−0.46	−3.9	−6.3	521	528	2.4
PDI-8Br$_2$	−0.36	−4.0	−6.3	520	541	2.3
PDI-F	−0.33	−4.1	−6.4	524	532	2.3
PDI-8Cl$_4$	−0.25	−4.2	−6.5	514	543	2.3
PDI-FBr$_2$	−0.24	−4.2	−6.5	526	545	2.3
NDI-8CN	−0.22	−4.2	−7.2	386	392	3.0
PDI-FCl$_4$	−0.13	−4.3	−6.6	519	547	2.3
PDI-8CN$_2$	−0.06	−4.3	−6.7	522	533	2.4
PDI-FCN$_2$	+0.03	−4.5	−6.8	523	532	2.3
NDI-8CN$_2$	+0.08	−4.5	−7.5	380	446	3.0

[a] 0.1 M TBAPF$_6$ in CH$_2$Cl$_2$: vs SCE. [b] Estimated vs vacuum level from $E_{LUMO} = 4.4$ eV − E_{red1}. [c] Estimated from HOMO = LUMO[b] − E_g. [d] From optical absorption/emission data in dichloromethane. E_g = optical gap.

electrochemical techniques,[97−99] and HOMO energies were estimated from the optical gaps (E_g) determined from the overlap of the normalized UV−vis and PL spectra (Figure S1). These data are summarized in Table 1.

An incremental displacement of the reduction potentials to more positive values correlates with increasing relative energetic ease of negatively charging a species in solution and, thus, the relative stability of the electron charge carriers in the solid state. The electrochemically derived LUMO energies, central to n-type charge transport characteristics, vary substantially and systematically across the series from PDI-8 (−0.46 V vs SCE) to NDI-8CN$_2$ (+0.08 V vs SCE), which is consistent with the number of arylene-core electron-withdrawing substituents and their respective Hammett coefficients.[100] Importantly, *N,N′*-functionalization with 1*H*,1*H*-perfluorobutyl groups only decreases the reduction potential by ∼ −0.13 V relative to the *N,N′*-*n*-octyl derivative, which should allow us to make comparisons between air stability due to fluorination (packing) and air stability due to orbital energetics.

Electronic structure calculations were employed to estimate molecular geometries due to the difficulty in obtaining diffraction-quality crystals for many members of the series and as further confirmations of the experimentally derived orbital energetic trends in this semiconductor series. The gas-phase energetics of the molecules presented here were calculated by DFT at the B3LYP level with a 6-31G* basis set in Spartan PC. The computed energies reported are for *N,N′*-dimethyl (R = Me) models, geometry-optimized with semiempirical PM3, followed by DFT/B3LYP/631-G* geometry optimization. Calculated in this manner, we find the LUMO energy versus vacuum to be −3.46 eV for the PDI-R-core, −3.62 eV for the PDI-RBr$_2$-core, −3.73 eV for the PDI-RCl$_4$-core, −3.85 eV for the NDI-RCN-core, −4.10 eV for the PDI-RCN$_2$-core, and −4.27 for the NDI-RCN$_2$-core. These LUMO energies obtained from the calculations are generally in close agreement with the experimental trends in reduction potentials (Table 1).

(97) Cervini, R.; Li, X.-C.; Spencer, G. W. C.; Holmes, A. B.; Moratti, S. C.; Friend, R. H. *Synth. Met.* **1997**, *84*, 359−360.
(98) Li, Y.; Cao, Y.; Gao, J.; Wang, D.; Yu, G.; Heeger, A. J. *Synth. Met.* **1999**, *99*, 243−248.
(99) Smestad, G. P.; Spiekermann, S.; Kowalik, J.; Grant, C. D.; Schwarzberg, A. M.; Zhang, J.; Tolbert, L. M.; Moons, E. *Sol. Energy Mater.* **2003**, *76*, 85−105.
(100) Anslyn, E. V.; Dougherty, D. A. *Modern Physical Organic Chemistry*; University Science Books: Sausalito, CA, 2006.

Changes in the absorption/emission maxima from UV−visible absorption spectroscopy and photoluminescence spectroscopy can be utilized to confirm molecular orbital energetics and/or structural relationships in the solution-phase compounds (Table 1 and Figure S1). The shift in absorption maximum (λ_{abs}) for the core-substituted perylenes reflects both the degree of conjugation in the perylene-core and the electron-withdrawing nature of the substituents. PDI-8, PDI-8Br$_2$, and PDI-8CN$_2$ have nearly identical λ_{abs} values of 521, 520, and 522 nm respectively, which reflects the relatively constant optical transition energy. The blue shift relative to PDI-8 of PDI-8Cl$_4$ to λ_{abs} of 514 nm reflects the severe distortion of the perylene core by the four chloro substituents, which results in an energetic increase in the optical transition. Similarly, the fluorinated derivatives exhibit similar trends with PDI-F, PDI-FBr$_2$, and PDI-FCN$_2$ exhibiting similar λ_{abs} values of 524, 526, and 523 nm, respectively. PDI-FCl$_4$ shows a blue shift to 519 nm relative to PDI-F, a similar shift compared to the *n*-octyl case. In comparing the *n*-octyl substituted vs 1*H*,1*H*-perfluorobutyl substituted materials, the fluorinated materials exhibit a similar 4 nm (PDI-R), 6 nm (PDI-RBr$_2$), and 4 nm (PDI-RCl$_4$) red shift relative to the *n*-octyl materials, most likely due to the slight LUMO energy depression upon addition of the electron-withdrawing fluorous chains. The PDI-RCN$_2$ derivatives show negligible λ_{abs} shifts upon fluorination.

The Stokes shift between the absorption and emission spectrum maxima of a molecule reflects the ability of the excited state to reorganize to a lower energy state prior to photoemission, and thus more rigid molecules tend to have smaller Stokes shifts.[101] The Stokes shifts here are found to have little dependence on the *N,N′*-substitution, with derivatives of similar cores only showing ∼1−2 nm differences in Stokes shifts. However, core substitution has a larger effect on Stokes shifts with relatively rigid PDI-R and PDI-RCN$_2$ cores showing small shifts of ∼7 and ∼10 nm, respectively. The slightly larger shift of the PDI-RCN$_2$ derivative reflects the small perylene-core distortion introduced upon cyanation, as elaborated upon in the Discussion. In contrast, the halogenated derivatives exhibit much larger shifts of ∼20 nm (PDI-RBr$_2$) and ∼29 nm (PDI-RCl$_4$), which reflects the greater excited-state reorganization of the more distorted perylene cores.

Thin Film X-ray Diffraction. X-ray diffraction experiments are crucial to understanding microstructure−function relationships between ordering over various length scales in organic thin films and charge transport properties. Conventionally, $\Theta/2\Theta$ diffraction scans are utilized to obtain out-of-plane *d*-spacings in the films, which allows determination of the molecular orientations relative to the substrate surface. In most bottom-gate OFET configurations, the optimal orientation for efficient charge transport between source and drain electrodes requires that the π-conjugated cores be aligned approximately perpendicular to the dielectric surface.[3,7] Additionally, the presence of multiple Bragg reflections and Laue oscillations around the first-order diffraction peak provides information regarding long-range film order, which in turn indicates the crystalline quality of these polycrystalline organic thin films.[102,103] Finally, rocking

(101) Turro, N. J. *Modern Molecular Photochemistry*; University Science Books: Sausalito, CA, 1991.
(102) Cullity, B. D.; Stock, S. R. *Elements of X-Ray Diffraction*; Prentice Hall: Upper Saddle River, NJ, 2001; p 664.
(103) Dürr, A. C.; Schreiber, F.; Munch, M.; Karl, N.; Krause, B.; Kruppa, V.; Dosch, H. *Appl. Phys. Lett.* **2002**, *81*, 2276−2278.
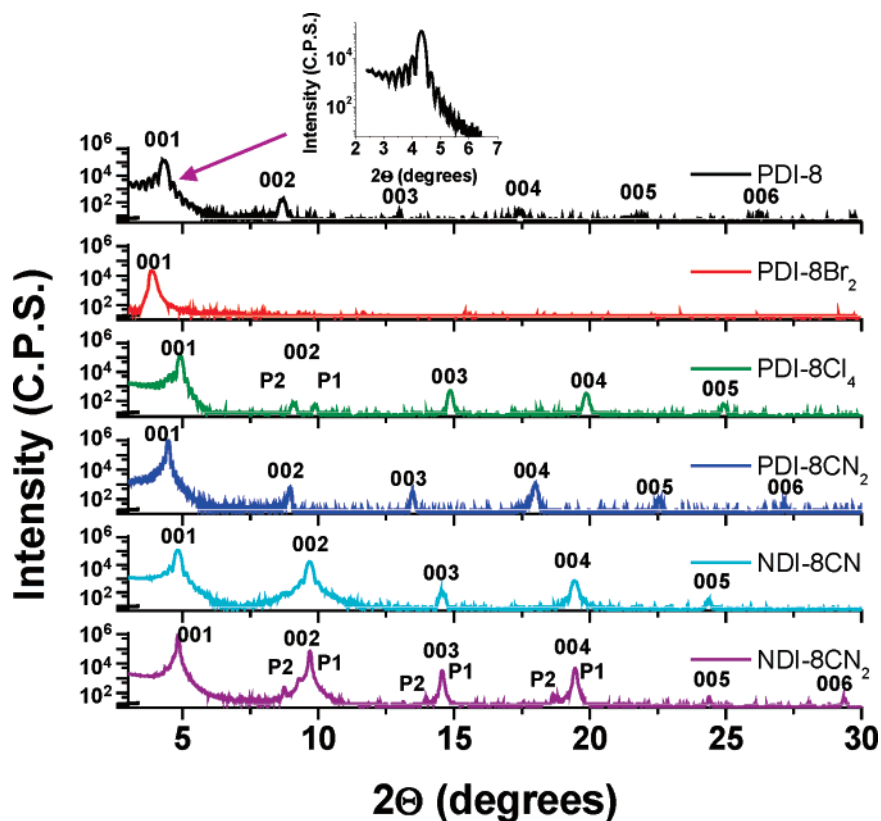
Figure 2. Representative $\Theta/2\Theta$ X-ray diffraction scans in logarithmic scale of vapor-deposited PDI-8 ($T_d = 130$ °C), PDI-8Br$_2$ ($T_d = 70$ °C), PDI-8Cl$_4$ ($T_d = 110$ °C), PDI-8CN$_2$ ($T_d = 130$ °C), NDI-8CN ($T_d = 130$ °C), and NDI-8CN$_2$ ($T_d = 110$ °C) films. The inset in the PDI-8 diffraction depicts a close-up of the Laue oscillations around the PDI-8 001 reflection. Also note the presence of other phases/orientations (P2) in addition to the primary phase (P1) in PDI-8Cl$_4$ and NDI-8CN$_2$ films. All plots have a break in the intensity axis between 10 and 20 C.P.S.; the scale is logarithmic at intensities above 20 C.P.S.

Table 2. Thin Film X-ray Diffraction Data for the Various Semiconductors of This Study, Indicating *d*-Spacing Related to the Molecular Long-Axis, Estimated Tilt Angle of the Semiconductor Relative to the Substrate Plane Normal, and Rocking Curve Full Width at Half-Maximum

semiconductor	T_d (°C)	d-spacing (Å)	tilt angle (deg)	ω_{fwhm}(001) (deg)
PDI-8	130	20.8	43	0.03
PDI-8Br$_2$	70	22.8	48	0.06
PDI-8Cl$_4$[a]	110	18.0 (19.4)	36 (40)	0.03 (0.03)
PDI-8CN$_2$	130	19.8	41	0.03
NDI-8CN	130	18.2	44	0.03
NDI-8CN$_2$[a]	110	18.2 (20.2)	44 (50)	0.03 (0.03)
PDI-F	130	16.1	45	0.03
PDI-FBr$_2$	130	15.5	43	n/a
PDI-FCl$_4$	130	n/a	n/a	n/a
PDI-FCN$_2$	130	19.5	59	0.05

[a] Minority phases are reported in parentheses.

curves evaluate the out-of-plane texturing in the films. All samples exhibit diffraction features in the $\Theta/2\Theta$ scans as depicted in Figure 2, while data are compiled in Table 2.

The present XRD data for the *n*-octyl derivatives indicate highly ordered/layered microstructures in all films,[6] which are grown on Si/SiO$_2$ by high vacuum physical vapor deposition at relatively slow growth rates (0.2 Å/s) and at elevated substrate temperatures (T_d). From the *d*-spacings calculated in these experiments, molecular tilt angles of ~45° are estimated from the PM3 geometry-optimized molecular lengths of PDI-8 (30.3 Å) and NDI-8 (26.3 Å). This value reasonably assumes the same basic crystal structures established for straight chain-substituted arylene diimides, such as *N,N'*-*n*-pentyl-PDI, NDI-F, and PDI-FCN$_2$, with negligible interdigitation of the *N,N'*-R^H/R^F chains

between arylene diimide layers.[31,104] Exceptions are PDI-8Cl$_4$ and NDI-8CN$_2$ films which contain a second thin film phase or orientation having a slightly larger *d*-spacing. Since crystal structures of the *n*-octyl derivatives are not known, the family of diffraction peaks are assumed to be 00*l* as assigned in other *n*-alkyl PDIs on the basis of single-crystal diffraction data of PDI-5.[43,71,85]

In addition to providing information on molecular orientation, XRD techniques were utilized to elucidate the microstructural quality of the polycrystalline thin films. The occurrence of (00*l*) progressions is indicative of long-range ordering,[103,105] and all films, except the PDI-8Br$_2$ films, exhibit five or more reflections for the sole or predominant phase. The PDI-8Br$_2$ films only exhibit a first-order reflection, meaning that the microstructural order is not comparable to that in the films of the other five *n*-octyl semiconductors. Rocking curves of the first-order reflections for all samples (Figure S3) indicate a high degree of texturing (fwhm ~0.03), meaning that the layers of the film microstructure are uniformly oriented relative to the substrate plane.[103,105] Again, films of PDI-8Br$_2$ exhibit substantially less texturing (fwhm ~0.06), further demonstrating the modest film quality. Finally, the Laue oscillations around the first-order diffraction peaks of PDI-8, PDI-8Cl$_4$, NDI-8CN, PDI-8CN$_2$, and NDI-8CN$_2$ films indicate that the crystallite spacings in the films are rather uniform,[103] and the spacing associated with the oscillations (~50 nm) indicates that the coherence is nearly uniform throughout the film thickness (~50 nm).

(104) Hadicke, E.; Graser, F. *Acta Crystallogr., Sect. C* **1986**, *42*, 189−195.
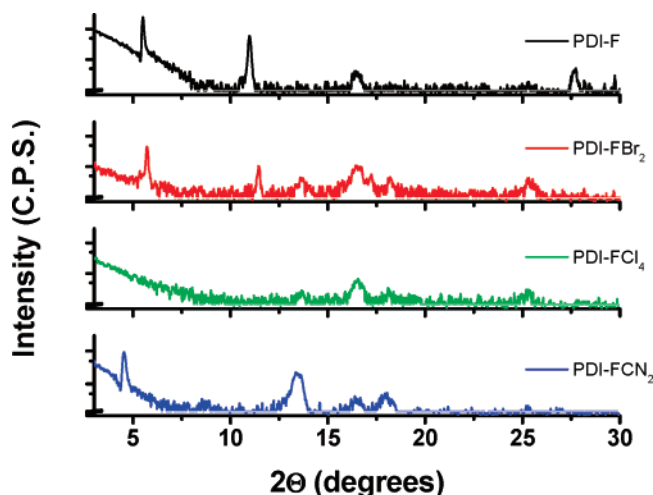(105) Wie, C. R. *Mater. Sci. Eng., R* **1994**, *R13*, 1−58.

Figure 3. Representative $\Theta/2\Theta$ X-ray diffraction scans in logarithmic scale of vapor-deposited PDI-F ($T_d = 130$ °C), PDI-FBr$_2$ ($T_d = 130$ °C), PDI-FCl$_4$ ($T_d = 130$ °C), and PDI-FCN$_2$ ($T_d = 130$ °C) films. All plots have a break in the intensity axis between 10 and 20 C.P.S.; the scale is logarithmic at intensities above 20 C.P.S.

Thin film XRD measurements on the 1*H*,1*H*-perfluorobutyl materials (Figure 3) reveal strikingly different film microstructures compared to the *n*-octyl substituted materials. The molecular orientation in these materials relative to the substrate was estimated assuming a molecular long-axis length of 22.8 Å, taken from the crystal structure of PDI-FCN$_2$.[31] Given the *d*-spacings in the thin films, PDI-F and PDI-FBr$_2$ have ~45° tilt angles with respect to the substrate, similar to the *n*-octyl materials. PDI-FCN$_2$ exhibits a slightly larger *d*-spacing, and thus the molecular tilt angle is nearly 60° relative to the substrate. The diffraction peaks associated with PDI-FCl$_4$ are at significantly larger 2Θ values compared to all other materials, and the lack of crystal structure data makes unambiguous assignment of these diffraction peaks problematic.

The out-of-plane film quality as evaluated by thin film XRD is significantly poorer for 1*H*,1*H*-perfluorobutyl materials compared to *n*-octyl materials. The diffraction peak intensity is noticeably less for these materials. Furthermore, the film microstructure appears more complex for the core substituted and fluorinated materials. PDI-F films exhibit one family of four reflections ($2\Theta = 5.5°$, 10.9°, 16.5°, and 27.6°) that likely correlate with the molecular long axis, whereas PDI-FBr$_2$, PDI-FCl$_4$, and PDI-FCN$_2$ exhibit multiple families of diffraction features suggestive of different phases or orientations. PDI-FBr$_2$ and PDI-FCN$_2$ films exhibit a family of peaks similar to those in PDI-F which correlate with the molecular long axis; however, these two semiconductors also exhibit reflections around $2\Theta = 13.5°$ and 18.0°, respectively. Note that PDI-FCl$_4$ films do not exhibit a diffraction peak at $2\Theta \approx 5°$ that corresponds to the molecular long axis, and PDI-FCl$_4$ films only exhibit reflections at $2\Theta = 13.5°$, 16.5°, 18.0°, and 25.3°, which are also observed in PDI-FBr$_2$ films. In films of these materials, there are no Laue oscillations associated with the diffraction peaks. In films of all the fluorocarbon-substituted materials, there are at least two families of diffraction features observed, which may correspond to different phases/orientations.

Thin Film Morphology by Atomic Force Microscopy. Characterization of the thin film microstructure at the substrate–thin film interface, the active region for charge transport in OFETs,[3] is challenging by conventional techniques; therefore, scanning probe microscopies are often used to evaluate the thin film surface morphology as an approximation to the active region at the interface with the dielectric.[4,106] AFM characterization of the semiconductor films grown in the present study reveals highly crystalline surface microstructures for PDI-8, PDI-8Cl$_4$, NDI-8CN, PDI-8CN$_2$, and NDI-8CN$_2$ (Figure 4). The surface morphologies of PDI-8, PDI-8CN$_2$, and NDI-8CN$_2$ films have similarly structured ribbon-like grains, while NDI-8CN and PDI-8Cl$_4$ films exhibit plate-like grains. The unique surface morphology of PDI-8Br$_2$ does not appear to be as crystalline or as smooth as that of the other films, with large features protruding from the film. In contrast, there are few discontinuous surface features for PDI-8, PDI-8Cl$_4$, and PDI-8CN$_2$. Since there is no evidence in the XRD for multiple phases or orientations in the films when these surface features are present, the microstructural/morphological origin of these growth features presumably does not involve additional phases or growth orientations.

The surface morphologies of PDI-F, PDI-FBr$_2$, PDI-FCl$_4$, and PDI-FCN$_2$ films appear substantially different from those of the *n*-octyl substituted materials (Figure 5). In the case of PDI-F and PDI-FBr$_2$, the films exhibit large crystal-like features protruding from the thin films, most similar to the PDI-8Br$_2$ case in the *n*-octyl materials. PDI-FCl$_4$ films exhibit an unusual honeycomb-like surface morphology, consistent with the unique XRD pattern also observed. PDI-FCN$_2$ forms smooth uniform films with only a few smaller crystals/protrusions; however, the surface morphology is substantially different from the *n*-octyl case.

Field-Effect Transistor Characterization. Organic field-effect transistors provide a simple device structure that allows detailed analysis of materials charge transport characteristics via evaluation of the current–voltage response. The function of the OFET is to modulate the semiconductor conductivity between the source and drain electrodes as a function of the gate voltage. A top-contact/bottom-gate configuration device in which the source and drain are vapor-deposited on top of the semiconductor film is used in this study (Figure 6a). When the bias (V_g) between the drain electrode (D) and the gate electrode (G) is 0.0 V, the transistor is "off" and little current should pass between source and drain. When V_g is applied, charges collect on either side of the dielectric, leading to an increase in the mobile n-type charge carrier density; hence current flows in the channel between source (S) and drain (D) electrodes when a source–drain bias (V_d) is applied. As a result, the current (I_d) between the S and D increases and the device is said to be "on". The performance parameters that can be extracted from the FET $I–V$ response curves include the charge carrier mobility (μ), current on–off ratio (I_{on}/I_{off}), and threshold voltage (V_{th}). These performance parameters are extracted within the assumptions of conventional transistor equations.[107] For organic transistors to become a viable technology, the component semiconductors must ideally have electrical properties as follows: $\mu \approx 0.1–1$ cm^2 V^{-1} s^{-1}, $V_{th} \approx 0$ V, and $I_{on}/I_{off} \approx 10^6$, with the availability of both environmentally stable p- and n-type

(106) DeLongchamp, D. M.; Sambasivan, S.; Fischer, D. A.; Lin, E. K.; Chang, P.; Murphy, A. R.; Frechet, J. M. J.; Subramanian, V. *Adv. Mater.* **2005**, *17*, 2340–2344.
(107) Sze, S. M. *Semiconductor Devices*; John Wiley & Sons: New York, 1985; p 523.
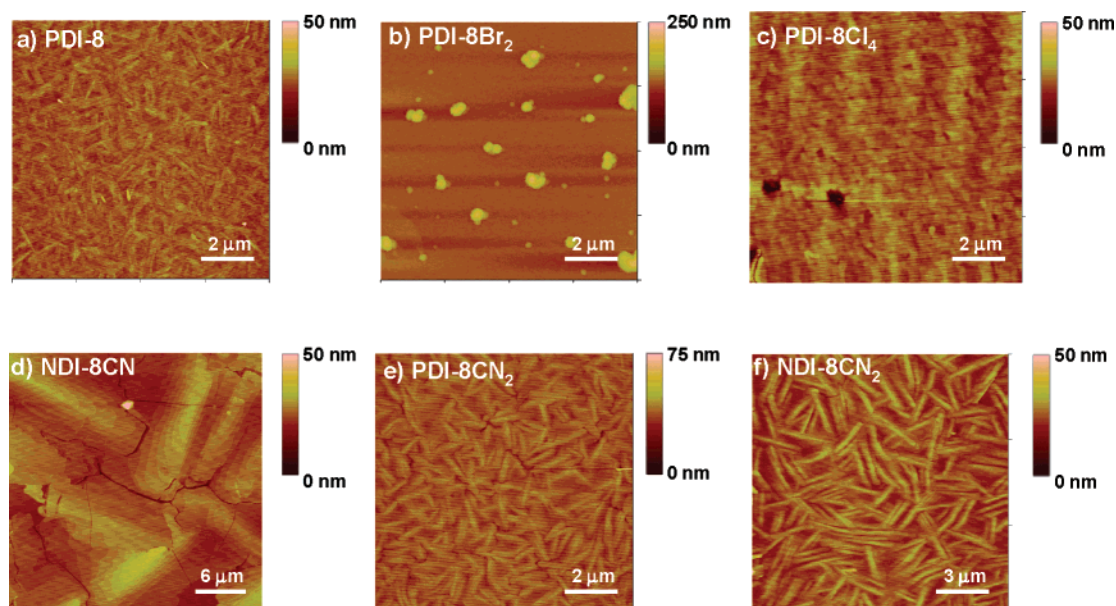
Figure 4. Tapping-mode AFM images of (a) PDI-8 (T_d = 130 °C), (b) PDI-8Br$_2$ (T_d = 70 °C), (c) PDI-8Cl$_4$ (T_d = 110 °C), (d) NDI-8CN (T_d = 130 °C), (e) PDI-8CN$_2$ (T_d = 130 °C), and (f) NDI-8CN$_2$ (T_d = 110 °C) films. The surface morphologies of PDI-8, PDI-8CN$_2$, and NDI-8CN$_2$ films are similar with ribbon-like grains. The surface morphology of PDI-8Cl$_4$ and NDI-8CN films exhibit plate-like grains. PDI-8Br$_2$ film morphology features a smooth background with protruding surface structures.
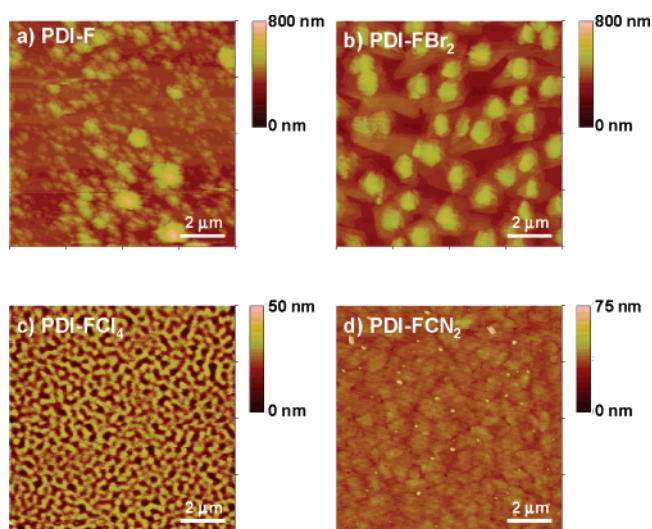

Figure 5. Tapping-mode AFM images of (a) PDI-F (T_d = 130 °C), (b) PDI-FBr$_2$ (T_d = 130 °C), (c) PDI-FCl$_4$ (T_d = 130 °C), and (d) PDI-FCN$_2$ (T_d = 130 °C) films.

semiconductors for organic-CMOS.[1,6,9,41,108] For the devices described below, the gate is highly doped silicon, while the dielectric is 300 nm SiO$_2$. The S/D contacts are gold. While silanol groups on SiO$_2$ dielectrics have been shown to act as electron traps for materials with E_{red1} < ∼ −0.6 V vs SCE,[58,109] the molecular energetics of the semiconductors with E_{red1} > −0.5 vs SCE utilized in this study should minimize trapping contributions from these functionalities. OFET parameters (μ, V_{th}, I_{on}/I_{off}) are averages of all measurements taken on the specified devices, and standard deviations are given only when greater than 5%. Transfer plots of I_d vs V_g were used to calculate the saturation mobility, threshold voltage, and current on−off

ratio for all devices. To compare the electrical properties across the series, all parameters were calculated for a V_d ensuring that the device was operating in the saturation regime (V_d > V_g).

***N*,*N*′-*n*-Octyl Substituted Arylene Diimide OFETs.** We first consider OFETs fabricated with thin films of the present *n*-octyl arylene diimides, deposited at the substrate temperatures (T_d's) indicated in Table 3, characterized under both vacuum and ambient atmosphere. We have chosen to discuss films deposited on bare SiO$_2$ at T_d's that yield the highest average carrier mobilities because dielectric surface treatments and unoptimized thin films give larger device-to-device variation. The electrical properties of the *n*-octyl semiconductor-based OFETs will first be discussed for operation under vacuum. Output plots showing I_d vs V_d for different gate biases measured under vacuum reveal that each material has well-defined linear and saturation regimes (Figure 6). Additionally, bidirectional transfer plots reveal minimal hysteresis for all nonhalogenated materials (Figure 7). The hysteresis of the dicyanated semiconductors is exceptionally small for n-channel OFETs. The two halogenated semiconductors, PDI-8Br$_2$ and PDI-8Cl$_4$, consistently exhibit the onset of the linear regime at V_d values positive of V_d = 0 V, which is usually indicative of non-ohmic contacts.[110]

The mobility trends in Table 3 reveal that PDI-8, PDI-8CN$_2$, and NDI-8CN$_2$ have the highest mobilities of 0.32, 0.13, and 0.15 cm^2 V^{-1} s^{-1}, respectively, while PDI-8Br$_2$, PDI-8Cl$_4$, and NDI-8CN have significantly lower mobilities ($\leq$10^{-3} cm^2 V^{-1} s^{-1}). These findings are generally in good agreement with previously published results for PDI-8[43,71] and cyano-PDI and -NDI derivatives.[31] For PDI-8Cl$_4$ films, the average electron mobility of 4 × 10^{-3} cm^2 V^{-1} s^{-1} is lower than those reported for other PDI-RCl$_4$-based semiconductors.[108,110] From microwave conductivity measurements (PR-TRMC) on bulk samples, a mobility of ∼0.14 cm^2 V^{-1} s^{-1} for an aryl-*n*-alkyl PDI-RCl$_4$

(108) *Printed Organic and Molecular Electronics*; Kluwer Academic Publishers: New York, 2004; p 695.
(109) Chua, L.-L.; Zaumseil, J.; Chang, J.-F.; Ou, E. C.-W.; Ho, P. K.-H.; Sirringhaus, H.; Friend, R. H. *Nature* **2005**, *434*, 194−199.

(110) Shen, Y.; Hosseini, A. R.; Wong, M. H.; Malliaras, G. C. *ChemPhysChem* **2004**, *5*, 16−25.
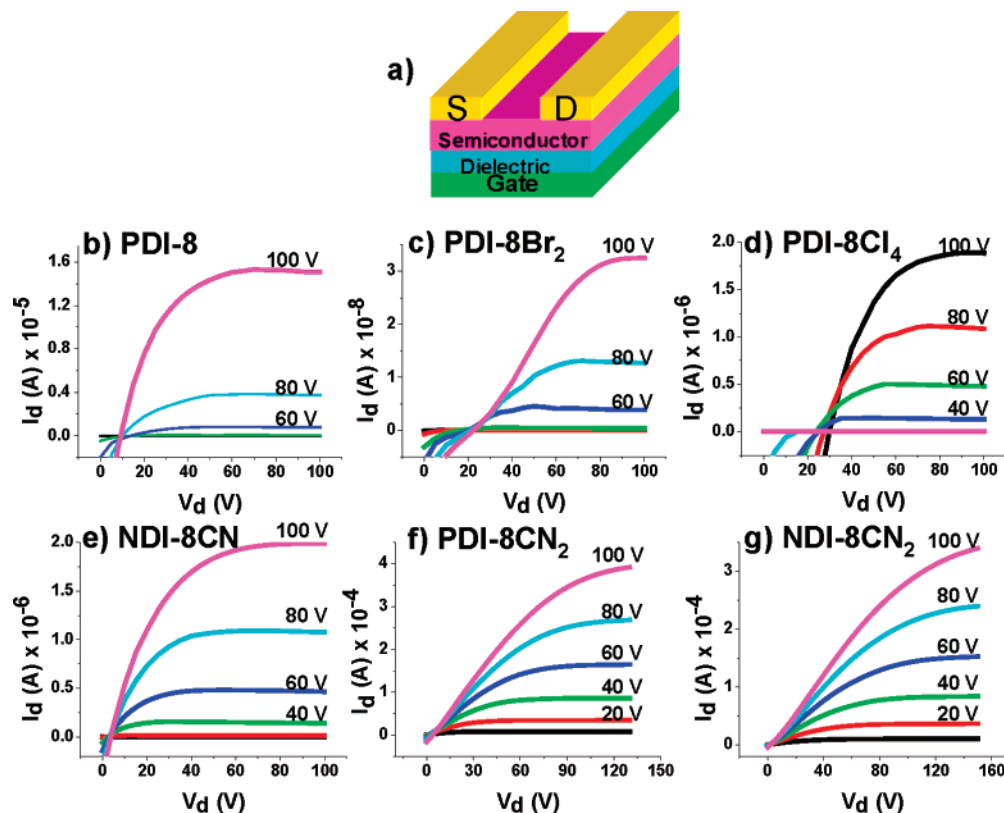
Figure 6. Representative OFET output characteristics of (a) PDI-8 ($T_d = 130$ °C), (b) PDI-8Br$_2$ ($T_d = 70$ °C), (c) PDI-8Cl$_4$ ($T_d = 110$ °C), (d) NDI-8CN ($T_d = 130$ °C), (e) PDI-8CN$_2$ ($T_d = 90$ °C), and (f) NDI-8CN$_2$ ($T_d = 110$ °C) films in a vacuum. Diagram (a) depicts a top-contact OFET geometry. The gate biases (V_g) are indicated immediately above the corresponding $I-V$ curves.

Table 3. OFET Electrical Properties with Standard Deviations for the Present Arylene Diimide Semiconductor Series Measured in Vacuum or Air on a Si/SiO$_2$ Substrate[a]

		vacuum			air		
semiconductor	T_d (°C)	μ (cm^2 V^{-1} s^{-1})	V_{th} (V)	I_{on}/I_{off}	μ (cm^{2}V^{-1}s^{-1})	V_{th} (V)	I_{on}/I_{off}
PDI-8	130	0.32	55 (4)	10^5	$2 (9) \times 10^{-4}$	147 (6)	10^4
PDI-8Br$_2$	70	$3 (3) \times 10^{-5}$	62 (8)	10^3	$9 (10) \times 10^{-6}$	97 (40)	10^3
PDI-8Cl$_4$	110	4×10^{-3}	37 (3)	10^4	$5 (2) \times 10^{-5}$	95 (19)	10^2
PDI-8CN$_2$	130	0.13 (0.02)	−14 (3)	10^3	0.12	−21 (2)	10^3
NDI-8CN	130	$4.7 (0.4) \times 10^{-3}$	28 (2)	10^5	2.8×10^{-4}	165 (9)	10^3
NDI-8CN$_2$	110	0.15 (0.01)	−37 (2)	10^2	0.11 (0.01)	−55 (5)	10^3
PDI-F	130	$1.4 (0.2) \times 10^{-3}$	38 (2)	10^4	$9.5 (0.1) \times 10^{-4}$	30 (3)	10^4
PDI-FBr$_2$[a]	130	$1.4 (0.4) \times 10^{-3}$	13 (7)	10^3	$8.8 (0.2) \times 10^{-4}$	28 (11)	10^2
PDI-FCl$_4$[a]	130	$2.8 (0.1) \times 10^{-5}$	25 (2)	10^3	$1.1 (0.2) \times 10^{-5}$	41 (16)	10^2
PDI-FCN$_2$	130	0.27 (0.09)	−22 (4)	10^3	0.24 (0.07)	−19 (3)	10^3

[a] Electron carrier mobility (μ) is given in cm^2 V^{-1} s^{-1}, and threshold voltages (V_{th}) are given in V. For the present dicyano semiconductors, current on−off ratios (I_{on}/I_{off}) are given for V_g (+100 V/−100 V) under both vacuum and air. For all other semiconductors, I_{on}/I_{off} for vacuum operation are for V_g (+100/−100 V) and for air V_g (+200 V/0 V). If standard deviations are less than 5%, they are not reported. [b] Device parameters reported here are for films grown on hexamethyldisilazane vapor-treated substrates because films grown on bare SiO$_2$ did not yield active OFETs.

has been reported.[111] These measurements, unlike OFETs, include coulombic interactions between electrons and holes and are not influenced by contacts and dielectric/thin film interface charge trapping, which reasonably explains the difference.[112] Moreover, *N*-H functionalized PDI-RCl$_4$ derivatives show similarly low electron mobilities (10^{-5}–10^{-3} cm^2 V^{-1} s^{-1}) on unfunctionalized SiO$_2$ substrates.[113] The carrier mobilities for the four perylene diimide semiconductors are best explained by slight differences in crystal packing and thin film quality as

discussed below. The mobility of the naphthalene diimide-based films will be discussed within the context of XRD, AFM, and calculated molecular geometries.

The threshold voltage (V_{th}) is used to evaluate the gate bias (V_g) at which electron trap states have been filled and the carriers become mobile. V_{th} exhibits device-to-device variations characteristic of OFETs, which can be influenced by many factors including materials purity, atmosphere during operation, film morphology, surface dipoles, film thickness, and light exposure.[55,69,85,114−116] Generally speaking, the V_{th} of the *n*-octyl

(111) Würthner, F.; Stepanenko, V.; Chen, Z.; Saha-Möller, C. R.; Kocher, N.; Stalke, D. *J. Org. Chem.* **2004**, *69*, 7933−7939.
(112) Warman, J. M.; de Haas, M. P.; Dicker, G.; Grozema, F. C.; Piris, J.; Debije, M. G. *Chem. Mater.* **2004**, *16*, 4600−4609.
(113) Ling, M.-M.; Erk, P.; Gomez, M.; Koenemann, M.; Locklin, J.; Bao, Z. *Adv. Mater.* **2007**, *19*, 1123−1127.

(114) Horowitz, G.; Hajlaoui, R.; Bouchriha, H.; Bourguiga, R.; Hajlaoui, M. *Adv. Mater.* **1998**, *10*, 923−927.
(115) Pernstich, K. P.; Goldmann, C.; Krellner, C.; Oberhoff, D.; Gundlach, D. J.; Batlogg, B. *Synth. Met.* **2004**, *146*, 325−328.
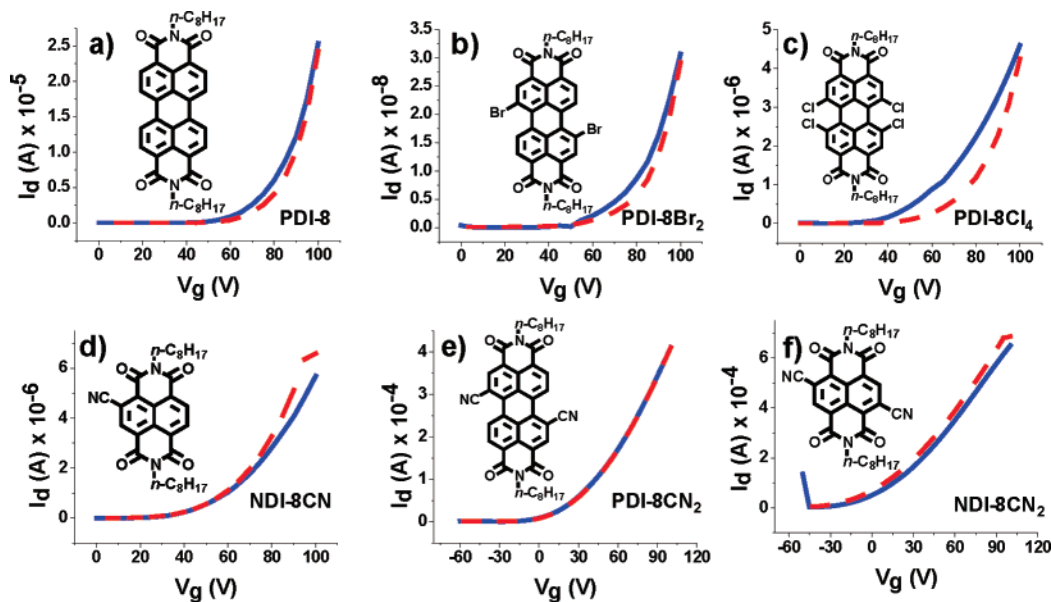
Figure 7. Bidirectional transfer plots for OFETs fabricated from films of (a) PDI-8 ($T_d = 130$ °C), (b) PDI-8Br$_2$ ($T_d = 70$ °C), (c) PDI-8Cl$_4$ ($T_d = 110$ °C), (d) NDI-8CN ($T_d = 130$ °C), (e) PDI-8CN$_2$ ($T_d = 90$ °C), and (f) NDI-8CN$_2$ ($T_d = 110$ °C) OFETs operated under vacuum. The solid blue trace is the positive V_g sweep, and the dotted red trace is the reverse V_g sweep.

semiconductor films systematically shifts more negative as the molecule becomes thermodynamically easier to reduce, indicated by a positive shift in reduction potential, as seen in Table 3 and Figure 9.

Current on−off ratios are used to characterize the efficiency with which the device can modulate current flow between the S and D contacts. The I_{on}/I_{off} ($V_g = +100$ V/-100 V) ratio is generally $\sim 10^4 - 10^5$ for PDI-8, PDI-8Cl$_4$, and NDI-8CN cases. PDI-8Br$_2$, PDI-8CN$_2$, and NDI-8CN$_2$ exhibit a lower I_{on}/I_{off} ratio of $\sim 10^3$. The relatively low I_{on}/I_{off} values are common for high electron affinity materials,[21,31,54,78] which often require taking the I_{on}/I_{off} for enhancement−depletion mode operation ($V_g < 0$ V/$V_g > 0$ V) to achieve values comparable to low electron affinity materials.[31,54] The primary reason for the low I_{on}/I_{off} is the substantial current flow at $V_g = 0$ V. In this semiconductor series, the I_d at $V_g = 0$ V is $\sim 10^{-12}$ A for PDI-8; $\sim 10^{-11}$A for PDI-8Br$_2$, PDI-8Cl$_4$, and NDI-8CN; $\sim 10^{-7}$ A for PDI-8CN$_2$; and $\sim 10^{-6}$ A for NDI-8CN$_2$.

All TFT characterization measurements performed in vacuum were also performed in ambient atmosphere. The measurements reported here are for exposure to air for 24 h after measurement under vacuum, although device electrical performance degradation for most of the present semiconductors is nearly instantaneous upon breaking vacuum. We will first consider the *n*-octyl functionalized materials. The output and bidirectional transfer plots for the semiconductors reveal relatively poor device response characteristics, with the exception of PDI-8CN$_2$ and NDI-8CN$_2$ (Figure 8). Since exposure to ambient atmosphere greatly increases the trap density in the films, extremely large gate biases are required to produce mobile charge carriers in the non-cyanated semiconductors (Table 3). The modest quality of the $I-V$ data is likely due to a combination of high trap density and physical degradation of the devices during operation under such extreme biases. The devices fabricated with PDI-8,

PDI-8Br$_2$, PDI-8Cl$_4$, and NDI-8CN films exhibit large response variabilities when operated in ambient atmosphere, doubtless in part due to the stress of the very high operating voltages and also in part due to variations in the way(s) that ambient atmosphere interacts with the films due to variations in film microstructure/morphology. Bidirectional transfer plots for all OFETs measured in air are shown in Figure 8. The hysteresis for all these semiconductors is dramatic indicating substantial charge trap densities, with the exception of PDI-8CN$_2$ and NDI-8CN$_2$. The hysteresis of PDI-8CN$_2$ devices in air is negligible while NDI-8CN$_2$ has small hysteresis, similar to the OFET response in vacuum.

Comparing the ambient atmosphere mobilities of the different semiconductors examined in this study, the PDI-8CN$_2$ and NDI-8CN$_2$ OFET mobilities are approximately 2−3 orders of magnitude greater than those of the other *n*-octyl materials. Upon exposure to air, the average mobility decreases by a factor of $1600\times$ for PDI-8, $3\times$ for PDI-8Br$_2$, $80\times$ for PDI-8Cl$_4$, and $17\times$ for NDI-8CN (Table 3). Contrastingly, changes to the PDI-8CN$_2$ carrier mobility in air are negligible within the standard deviation, while NDI-8CN$_2$ mobilities decrease by a factor $1.4\times$ upon air exposure. The relatively small decrease in mobility of PDI-8Br$_2$ reflects the modest film quality as evidenced by the XRD and AFM data, and which results in poor semiconductor performance under vacuum as well. Thus, the inclusion of ambient-atmosphere-based traps does not substantially alter the trap density magnitude relative to that under vacuum.

The changes in V_{th} for samples in air compared to devices characterized under vacuum are very large for all *n*-octyl semiconductors except PDI-8CN$_2$ and NDI-8CN$_2$ (Table 3). In devices fabricated with films of PDI-8, PDI-8Br$_2$, PDI-8Cl$_4$, and NDI-8CN, the V_{th} increases relative to vacuum operation by 92 ± 7, 35 ± 41, 58 ± 19, and 137 ± 9 V, respectively, upon exposure to ambient atmosphere. The huge variation associated with PDI-8Br$_2$ is probably due to the poor film quality as reported in the XRD, AFM, and Discussion sections. The V_{th} decreases slightly (<10 V) relative to vacuum operation in

(116) Pernstich, K. P.; Haas, S.; Oberhoff, D.; Goldmann, C.; Gundlach, D. J.; Batlogg, B.; Rashid, A. N.; Schitter, G. *J. Appl. Phys.* **2004**, *96*, 6431−6438.
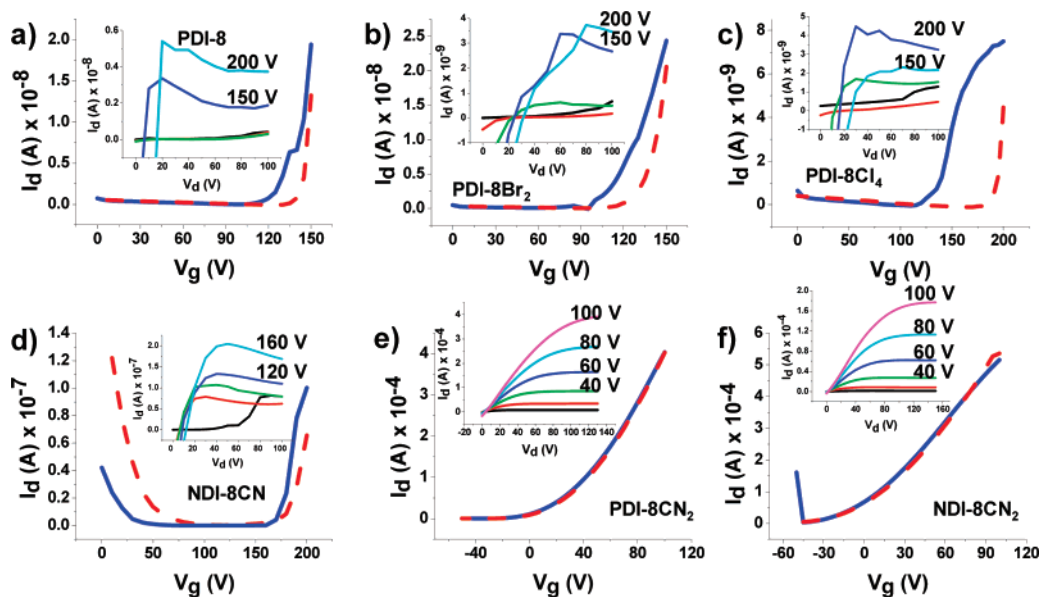
Figure 8. Bidirectional transfer plots and output plots (insets) for OFETs fabricated from films of (a) PDI-8 ($T_d = 130$ °C), (b) PDI-8Br$_2$ ($T_d = 70$ °C), (c) PDI-8Cl$_4$ ($T_d = 110$ °C), (d) NDI-8CN ($T_d = 130$ °C), (e) PDI-8CN$_2$ ($T_d = 130$ °C), and (f) NDI-8CN$_2$ ($T_d = 110$ °C) measured in ambient atmosphere, demonstrating the stability of PDI-8CN$_2$. The gate bias (V_g) in the output plots is indicated directly above the corresponding I–V trace. The solid blue trace of the bidirectional transfer plot is the positive V_g sweep, and the dashed red trace is the reverse V_g sweep.
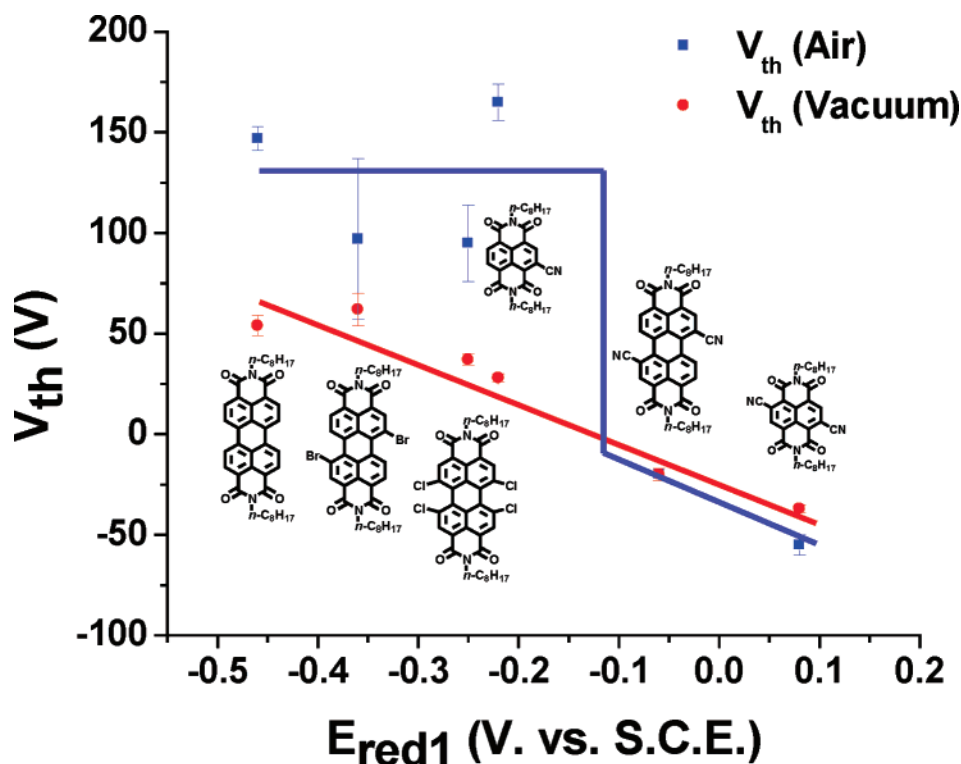

Figure 9. V_{th} for optimized OFETs of the indicated materials with standard deviations as a function of electrochemical reduction potential. The decrease in V_{th} (vacuum) with positive E_{red1} shift demonstrates increasing ease of charge carrier generation with increased ease of reduction. The red and blue lines are drawn as guides to the eye. Additionally, the shift in threshold voltage from vacuum to air operation demonstrates that materials with $E_{red1} \geq \sim -0.1$ V exhibit the largest increases in trap densities due to their higher charge carrier energies.

PDI-8CN$_2$ and NDI-8CN$_2$-based devices, which is likely due to adventitious dopants common in high electron affinity materials.[31,54,83] The shift in threshold voltage from devices operated in vacuum vs ambient can be used to estimate, via established approaches,[85] the increase in trap density (N_t). Based on the shift in threshold voltage (Figure 9) for a given material, N_t is found to be $(6 \pm 0.5) \times 10^{13}$ cm^{-2} for PDI-8, $(2 \pm 2) \times 10^{13}$ cm^{-2} for PDI-8Br$_2$, $(4 \pm 1) \times 10^{13}$ cm^{-2} for PDI-8Cl$_4$,

and $(9 \pm 0.6) \times 10^{13}$ cm^{-2} for NDI-8CN. Similar to the other electrical parameters, while I_{on}/I_{off} is affected adversely by $\sim 10^2$ for air exposure in PDI-8, PDI-8Cl$_4$, and NDI-8CN devices, I_{on}/I_{off} ($V_g = -100$ V/100 V) for PDI-8CN$_2$ (10^3) and PDI-8Br$_2$ (10^3) are unchanged and NDI-8CN$_2$ exhibits a slightly higher current modulation of 10^4. The improvement of NDI-8CN$_2$ I_{on}/I_{off} upon air exposure likely reflects trapping of dopant-induced charge carriers giving lower I_{off}. The lack of change in
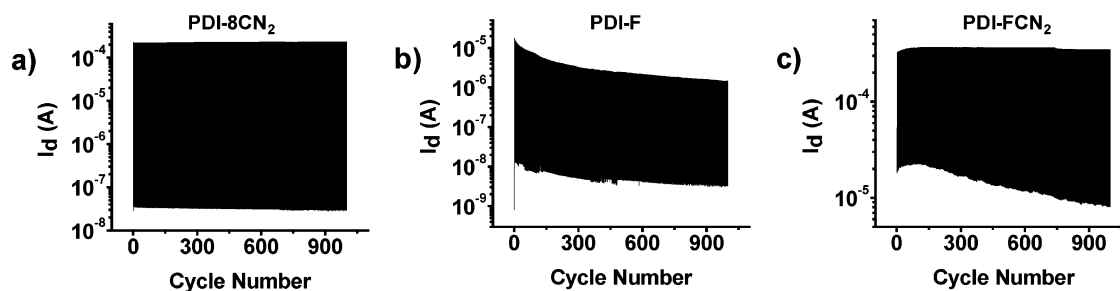
Figure 10. I_d at $V_d = +100$ V when the indicated OFET is cycled in air between (a) $V_g = -25$ V and $V_g = +100$ V for PDI-8CN$_2$, (b) $V_g = +25$ V and $V_g = +100$ V for PDI-F, and (c) $V_g = -25$ V and $V_g = 75$ V for PDI-FCN$_2$.

the I_{on}/I_{off} for PDI-8Br$_2$ reflects the poor quality of the semiconducting film leading to large trap densities in a vacuum; therefore, there is little change upon exposure to air, as will be discussed below.

***N,N′*-1*H*,1*H*-Perfluorobutyl Substituted Perylene Diimide OFETs.** As a comparison to the *n*-octyl functionalized materials, OFETs fabricated at $T_d = 130$ °C with films of the 1*H*,1*H*-perfluorobutyl-substituted perylene diimide semiconductors were evaluated in a vacuum and air. These analogues should exhibit fluorocarbon barrier-induced behavior similar to the previously reported air-stable naphthalene diimide materials, extensively studied by Katz et al., and the recently reported fluorophenyl-substituted materials of Bao and Furukawa et al.[48,62,63,77,79,80] The OFET data for the fluorinated materials are compiled in Table 3 and Figures S6 and S7. Importantly, and consistent with previously reported work, the 1*H*,1*H*-perfluorobutyl chain functionalization extends air-stable OFET operation to all these semiconductors, despite the small positive shift in reduction potential of $\sim +0.13$ V.

The electron carrier mobility in a vacuum of the 1*H*,1*H*-perfluorobutyl substituted semiconductors is significantly greater than the *n*-octyl counterparts for the disubstituted PDIs, PDI-FBr$_2$ ((3 ± 3) × 10^{-5} cm^2 V^{-1} s^{-1}) and PDI-FCN$_2$ ((0.27 ± 0.09) cm^2 V^{-1} s^{-1}).[117] In the case of PDI-F and PDI-FCl$_4$, the devices prepared with films of the fluoroalkyl material exhibit lower mobilities relative to the *n*-octyl derivative of (1.4 ± 0.2) × 10^{-3} cm^2 V^{-1} s^{-1} and (2.8 ± 0.1) × 10^{-5} cm^2 V^{-1} s^{-1}, respectively. The I_{on}/I_{off} ratios of OFETs fabricated with the R^F-substituted materials and measured in vacuum are 10^4 for PDI-F, 10^2 for PDI-FBr$_2$, 10^3 for PDI-FCl$_4$, and 10^3 for PDI-FCN$_2$. These numbers are generally lower than those for the *n*-octyl counterparts, with the exception of PDI-8CN$_2$/PDI-FCN$_2$ which show comparable I_{on}/I_{off} values.

The electrical parameters for the fluorocarbon series measured in air reveal that all four materials afford air-stable OFETs. Within the estimated standard deviations, the change in average electron mobility of the R^F-functionalized materials in air relative to vacuum are very small or negligible. Slight or statistically insignificant V_{th} shifts relative to vacuum operation are observed in the fluoroalkyl substituted semiconductor films upon exposure to ambient. Since these V_{th} shifts are insignificant, the increase in trap density upon exposure to ambient atmosphere vs vacuum are relatively small. I_{on}/I_{off} is lower by 1 order of magnitude for PDI-FBr$_2$ and PDI-FCl$_4$ in air, which have $I_{on}/I_{off} = 10^2$. I_{on}/I_{off} values for PDI-F and PDI-FCN$_2$ remain

unchanged in air vs vacuum with values of 10^4 and 10^3, respectively.

Durability Evaluation of *N,N′*-*n*-Octyl vs *N,N′*-1*H*,1*H*-Perfluorobutyl Semiconductor-Based TFTs. The durability of PDI-8CN$_2$, PDI-F, and PDI-FCN$_2$ TFTs operating under ambient conditions was investigated by cycling the devices in air for 1000 cycles ($\sim$1.5 h) immediately after breaking vacuum (Figure 10). Cycling PDI-8CN$_2$ devices between $V_g = -25$ V and $V_g = +100$ V reveals very stable source−drain on-currents (I_{on}) with an $\sim$10% (2×10^{-5} A) increase. PDI-F devices cycled between $V_g = +25$ V and $V_g = 100$ V exhibit exponential-like decay in I_{on} of $\sim$92% (2×10^{-5} A) over the test. PDI-FCN$_2$ devices cycled between $V_g = -25$ and 75 V exhibit very stable I_{on} with an $\sim$11% increase (4×10^{-5} A) over the measurement. These data indicate that the environmental stability of the PDI-F semiconductor is subject to substantial variation over time and operating cycles. Previously reported and promising air-stable n-type organic semiconductors containing fluorocarbon groups have also been reported to be fragile, with fluoroalkyl-NDI derivatives undergoing device failure after cycling in air, which was ascribed to contact delamination,[62] and F$_{16}$CuPc devices undergoing a marked mobility erosion over $\sim$1000 h.[56] In contrast, PDI-8CN$_2$ and NDI-8CN$_2$ devices stored in a laboratory ambient atmosphere over the course of 18 months exhibit slightly positive ($\sim$10 V) drifts in V_{th} and electron mobility $\approx$ 0.10 cm^2 V^{-1} s^{-1}. Additionally, previously reported PDI-FCN$_2$ devices[31] measured in air after more than 3 years of storage in ambient atmosphere exhibit transistor electron mobilities as high as 0.45 cm^2 V^{-1} s^{-1}.

Inspection of the device performance parameters at cycle 0 and 1001 for the three materials reveals minimal change for the two dicyanated derivatives. For the OFETs fabricated with a PDI-8CN$_2$ film, the electron mobility at cycle 0 and 1001 was 0.10 cm^2 V^{-1} s^{-1}, while, for the PDI−FCN$_2$ device, the carrier mobility was 0.2 cm^2 V^{-1} s^{-1} before and after the cycling. For the OFETs fabricated with a PDI-F thin film, the field-effect mobility decreases from 1.9×10^{-2} cm^2 V^{-1} s^{-1} before cycling to 1.4×10^{-2} cm^2 V^{-1} s^{-1} after cycling. The threshold voltage for the PDI-8CN$_2$ TFT reveals a negligible shift from -3 V before cycling to -2 V after cycling, while the PDI-FCN$_2$ TFT exhibits an increase from -26 V before cycling to -19 V after cycling. The shifts of 1 V for PDI-8CN$_2$ and 7 V for PDI-FCN$_2$ correspond to an $\sim 6 \times 10^{10}$ cm^{-2} and $\sim 4 \times 10^{11}$ cm^{-2} increase in trap density for both cases. The V_{th} for PDI-F devices, shifts from 47 V before cycling to 65 V after cycling, which corresponds to an increase in V_{th} of 18 V or in N_t of $\sim 1 \times 10^{12}$ cm^{-2}. The variation in current on−off ratios before and after cycling is generally negligible in all

(117) Note that PDI-FCN$_2$-based OFETs can exhibit electron mobilities as high as 0.6 cm^2 V^{-1} s^{-1} on hexamethyldisilazane (HMDS) treated substrates. However, surface treatments significantly shift V_{th}, one of the significant parameters in comparing materials within this study.
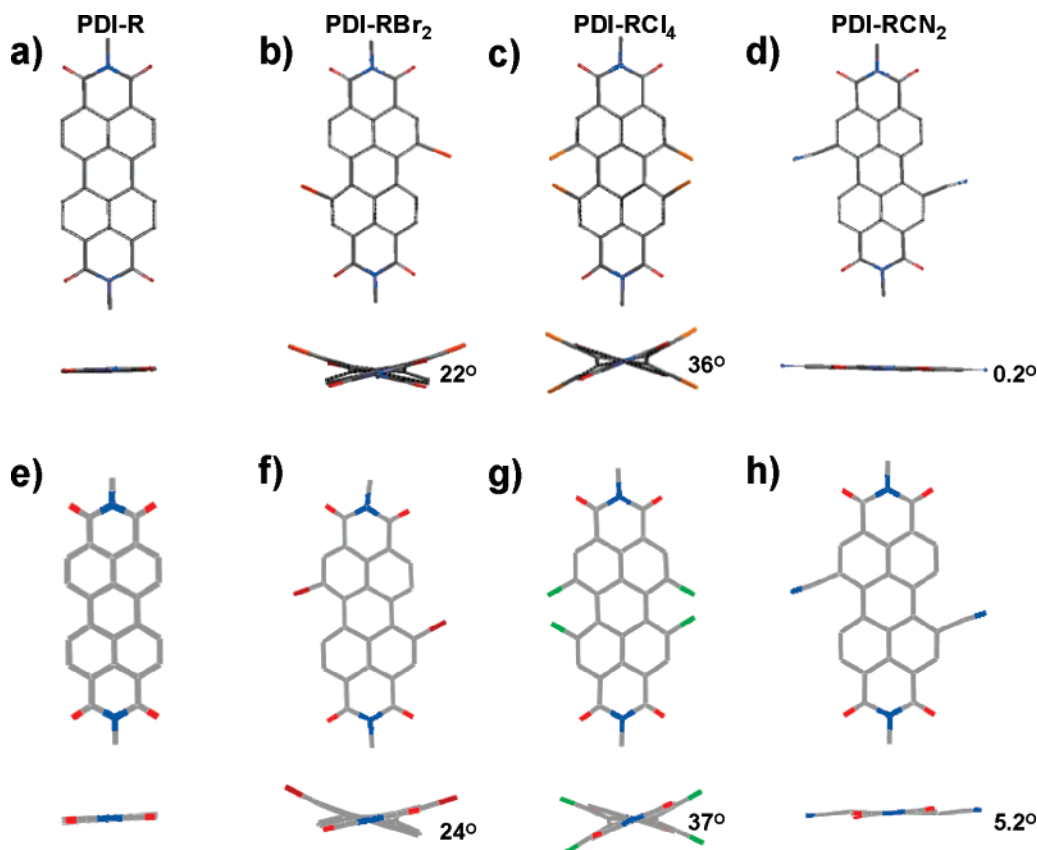
Figure 11. Molecular geometries of the four PDI cores investigated in this study. Structures a−d are derived from DFT calculations on *N,N′*-methyl derivatives (R = Me), while structures e−h are taken from previously published X-ray diffraction studies. The top projection is the face-on view of the molecule, and the view directly below is the view along the molecular long axis. The torsional angles between the mean-square planes of the two perylene core naphthalene units are shown.

three cases, with I_{on}/I_{off} for the PDI-F, PDI-8CN$_2$, and PDI-FCN$_2$ having values of 10^4, 10^3, and 10, respectively.

Discussion

Crystal Structure Analysis. Diffraction-quality single crystals of the specific arylene diimide derivatives investigated in this study have proven problematic to grow. However, the crystal structure of every perylene diimide *core* examined in this study has been previously reported,[31,87,88,104,111] and crystallographic data for derivatives having slightly different *N,N′*-substituents (R) were therefore employed as reasonable core models for PDI-8, PDI-8Br$_2$, PDI-8Cl$_4$, and PDI-8CN$_2$ (Figure 11). Unfortunately, there are no known crystal structures of core-cyanated naphthalene diimide materials, so the present discussion is restricted to perylene derivatives. In the crystal structures of the core-substituted PDIs, the differences in packing motif can be largely attributed to the introduction of intramolecular nonbonded repulsions and the torsional distortions in the PDI core which result. In the DFT-level calculations discussed earlier, the optimized molecular geometries of the cores are very similar to the core geometries found in the experimental crystal structures (Figure 11). Therefore, comparisons between the crystal packing of the present PDIs and those in the published crystal structures should be informative. Note that our interpretation of perylene core-substitution effects on solid-state packing is similar to the interpretation of PDI packing in

solution-phase aggregates of similarly core-substituted perylene diimides, confirming the importance of these relationships.[118]

Core Substitution Effects on Molecular Geometries. From the aforementioned crystal structures, it can be seen that core substitution of perylene diimides leads to torsion/buckling of the core as illustrated in Figure 11. The PDI-R perylene core is rigorously planar when unsubstituted; however when substitution is introduced at the 1, 6, 7, or 12 positions, the torsional angle (TA) between the two naphthalene mean-square planes of the PDI core increases to 5.2° for PDI-RCN$_2$, 24° for PDI-RBr$_2$, and 37° for PDI-RCl$_4$. The trend in TA distortion is paralleled by the trend in Stokes shift which increases as follows: PDI-R (7 nm), PDI-RCN$_2$ (10 nm), PDI-RBr$_2$ (20 nm), and PDI-RCl$_4$ (29 nm), reflecting significant excited-state reorganization in the more distorted PDI-RBr$_2$ and PDI-RCl$_4$ structures. Thus, nonbonded repulsions arising from the core substituents in the halogenated molecules leads to very large twisting at the central perylene C$_6$ core, and the relatively small cyano group induces significantly less distortion. Interestingly, the minor distortion of the cyano-substituted perylene core is accompanied by a decrease of the C(aromatic)−C−N bond angle from 180° to 173°, which partially relieves steric interactions with the proximate C(aromatic)−H group. Similar C−C−N angle compressions have been previously observed in *ortho*-substituted benzonitriles.[119]

(118) Chen, Z.; Baumeister, U.; Tschierski, C.; Würthner, F. *Chem.−Eur. J.* **2007**, *13*, 450−465.
(119) Britton, D.; Cramer, C. J. *Acta Crystallogr., Sect. C* **2006**, *C62*, o307−o309.
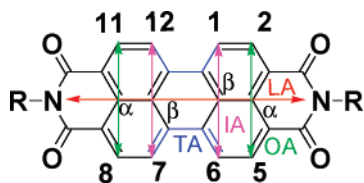
Figure 12. Molecular structure of PDI skeleton depicting atom numbering schemes and angles discussed. The long-axis (red LA) runs from N to N. The torsional angle (TA) between naphthalene units is taken from the four bay region carbons indicated in blue. The interior angles (magenta IA) and outer angles (green OA) across the perylene unit are also depicted.

Additional distortions of the naphthalene subunits in the substituted PDIs are also observed, in contrast to the planar geometry of the unsubstituted PDI-R skeleton (Figure 11a and 11e). In an undistorted perylene diimide, the naphthalene subunits should be planar. However, when the PDI skeleton is substituted, the naphthalene units fold slightly. We will define these folding angles in terms of the inner angles (IA), $\angle$ $C_1-C_\beta-C_6$ and $\angle$ $C_7-C_\beta-C_{12}$, while the outer angles (OA) are $\angle$ $C_2-C_\alpha-C_5$ and $\angle$ $C_8-C_\alpha-C_{11}$, Figure 12. In the case of PDI-RBr_2, the skeleton increasingly twists from the imide group toward the central C_6-unit with an OA distortion of 1.8° and an IA distortion of 3.2°. While the twist around the central C_6-unit of the PDI-RCl_4 core is severe, as discussed above, the distortion of the naphthalene rings is minimal with IA and OA distortions of 1.2°. Conversely, for PDI-RCN_2, the torsion around the central C_6-unit is minor, but the distortion of the naphthalene units is the most severe in this case, with an IA torsion of 4.9° and an OA torsion of 3.7°. Thus, the degree of IA and OA folding of the naphthalene subunits is inversely proportional to the torsional strain at the perylene central C_6 core.

The interplay between the substituent-derived steric-based strain at the central C_6 core vs that seen in the naphthalene subunits has interesting consequences for positioning of the substituents relative to the molecular planes. In PDI-RBr_2, because the naphthalene units remain relatively planar and the distortion is primarily associated with the central C_6-unit, the bromo substituents are displaced to the same side of the PDI plane, eliminating the molecular inversion center. Similarly in PDI-RCl_4, the chloro-substituents at positions 1,7 and 6,12 are displaced to the same side of the PDI plane. However, the symmetry of the tetra-substituted bay region does not lead to the asymmetry observed in PDI-RBr_2. For PDI-RCN_2, the relatively large distortion of the naphthalene units versus the central C_6 core results in the cyano substituents being displaced to opposite sides of the perylene plane, thus maintaining the molecular inversion center.

Core Substitution Effects on Crystal Packing. Upon examining the packing motifs of the four published PDI derivative crystal structures, the similarity between the unsubstituted and cyanated structures stands out (Figure 13). In both cases, the molecules are relatively planar with a slip-stacked packing arrangement, where the long axes (LAs) of the cores, defined by the N(imide)−N(imide) vector, are nearly in register relative to the LA of the adjacent molecule. Previous computational studies from this laboratory have already indicated that this packing motif is efficacious for efficient charge transport.[29]

In the case of PDI-RBr_2 and PDI-RCl_4, the highly distorted perylene skeletons reflect severe substituent-originated non-bonded repulsions in the bay-region (1, 6, 7, 12) positions

(Figure 12) and result in significantly altered packing relative to PDI-R and PDI-RCN_2 (Figure 13a and 13d). In the case of PDI-RBr_2 (Figures 13b), the molecular packing scheme is uniquely complicated due to less extensive segregation of the aromatic and alkyl sections of the semiconductor. Additionally, the location of the Br substituents on the same side of the PDI plane leads to dimer-like packing where the outlying bromine atoms allow close packing of an adjacent perylene unit on only one side. While PDI-RCl_4 forms a more continuous network (Figure 11c), the $\pi-\pi$ overlap between nearest neighbors is only between naphthalenic subunits rather than involving the entire molecular π-system.

In addition to alterations in the relative crystallographic molecular orientations, core substitution results in dramatic differences in intermolecular contacts. In the case of PDI-RCN_2 and PDI-R, the minimum interplanar spacing is ∼3.4 Å for both. The large PDI-RBr_2 bromine substituents induce the greatest interplanar spacing of 3.64 Å, and the smaller PDI-RCl_4 chlorine substituents lead to a closer packing (3.51 Å), despite a greater central C_6 core torsional angle (Figure 12). From these observations, it is evident that the design of core-substituted PDI-based semiconductors that maintain the advantageous crystal packing properties of the parent PDI molecule requires that the substituents be sterically unencumbering to minimize core torsion and consequently enhance intermolecular π overlap.

Carrier Mobilities of Substitued Arylene Diimides in a Vacuum. The differences in carrier mobilities in vacuum between the six *n*-octyl subject semiconductors can be explained primarily on the basis of molecular packing and film microstructural trends. PDI-$8Br_2$ is a particularly poor OFET material. The crystal structure suggests that the $\pi-\pi$ orbital overlap between adjacent PDI-RBr_2 cores is minimal because of the sizable intermolecular distances and the discontinuity of the "dimer"-based packing motif which should depress carrier mobility (Figure 13).[29,30] The weakness of the orbital overlap in the solid is also consistent with PDI-$8Br_2$ having the lowest melting point of the perylene-based semiconductors (Figure S2). The film microstructure as assessed by XRD shows that the crystalline quality/order of the PDI-$8Br_2$ film is unfavorable for efficient charge transport (Figure 2), as evidenced by the absence of higher-order diffraction peaks which would indicate long-range order and the relatively large fwhm values in the rocking curve, signifying poor out-of-plane texturing (Table 2 and Figure S3). Additionally, the film morphology assessed by AFM does not reveal the distinctive crystalline features associated with the other *n*-octyl derivative-based polycrystalline thin films examined in this study (Figure 4). The poor film quality and discontinuous molecular packing motif of this material are arguably the primary reasons for the substantially lower mobility observed in PDI-$8Br_2$-based OFETs. Additionally, the large degree of decomposition (∼20% residual mass) in the PDI-$8Br_2$ reduced pressure TGA (Figure S2) suggests that the OFET films are likely to contain decomposition products which may lead to trap states. To simplify subsequent data interpretation, PDI-$8Br_2$ will not be discussed further because the poor quality of the semiconductor growth leads to an erratic OFET response and likely large trap densities (N_t) even while operating under vacuum.

OFET carrier mobilities in PDI-$8Cl_4$ and NDI-8CN are also modest. The crystal structure of PDI-RCl_4 suggests that in-
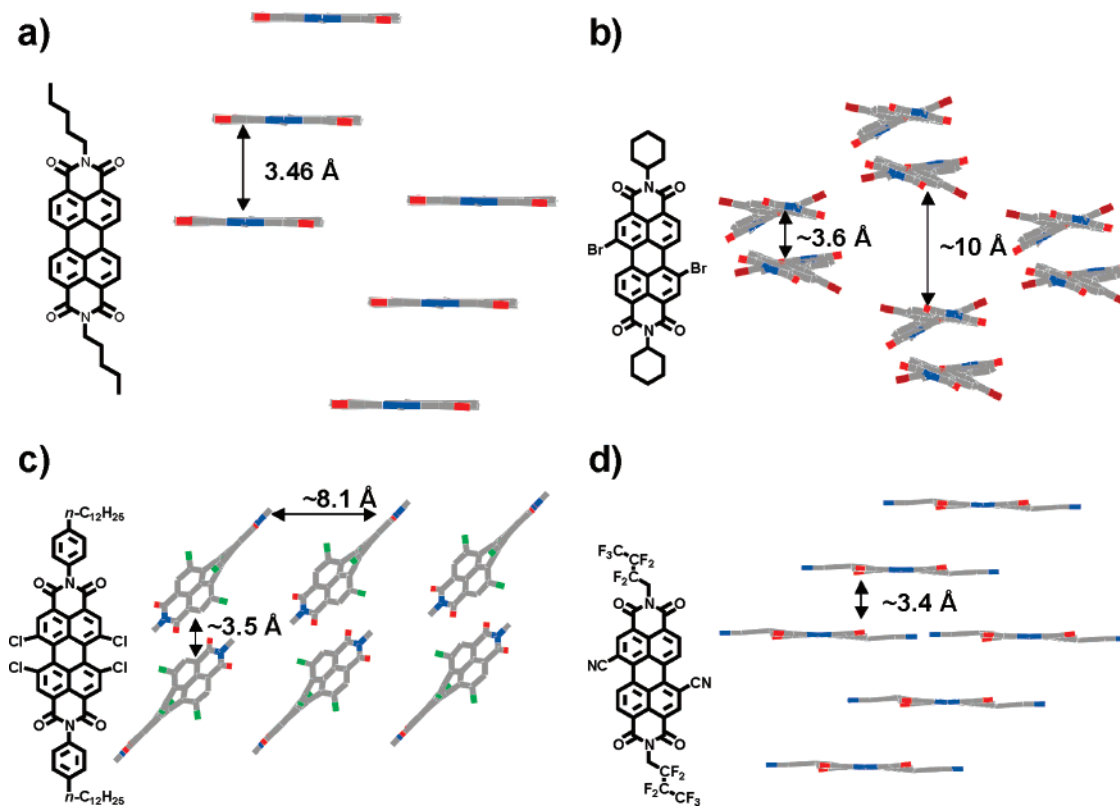
Figure 13. Crystal structures of (a) PDI-R,[78] (b) PDI-RBr$_2$,[66] (c) PDI-RCl$_4$,[65] and (d) PDI-RCN$_2$[26] showing the packing relationships among the four molecules. The molecular structure to the left of each packing diagram depicts the *N,N′* substituents for that particular crystal structure, which have been deleted for ease of viewing.

tramolecular π-orbital overlap is less than that in PDI-8 and PDI-8CN$_2$ because the intermolecular spacing is greater and molecular $\pi-\pi$ overlap is only between naphthalenic monoimide subunits rather than involving the entire PDI π-system (Figure 13). Additionally, the melting point of PDI-8Cl$_4$ is substantially lower than those of PDI-8 and PDI-8CN$_2$ (Figure S2), suggesting weaker intermolecular interactions. While PDI-8Cl$_4$ thin film morphology (Figure 4) and microstructure (Figures 2 and S3, and Table 2) are comparable to those of PDI-8 and PDI-8CN$_2$ films, the presence of two distinct phases/crystallographic orientations may depress mobility by creating trap states at the interfaces between phases/orientations.[120] Since crystal structure data on NDI-8CN has yet to be obtained, assumptions based on thin film XRD data are most relevant to explaining the low electron mobilities. The striking similarity in thin film XRD data between low mobility NDI-8CN and high mobility NDI-8CN$_2$ suggests that the difference in mobility is likely due to in-plane ordering. Assuming that the crystal structure of NDI-8CN packs in a layered motif with segregated aromatic and aliphatic regions, as suggested in the thin film XRD (Figure 2), the molecular overlap between NDI-8CN units is likely rather different from that between NDI-8CN$_2$ units.

The electron mobilities of PDI-8, PDI-8CN$_2$, and NDI-8CN$_2$ thin films measured in a vacuum are similar. The correlation between the high mobility of *N*-alkyl PDI materials and the excellent crystal packing/film-forming properties has been documented previously.[43,71,85] The similarities in the slip-stacked crystal packing motifs (Figure 13) and film morphologies/

microstructures as deduced by AFM (Figure 4) and XRD (Figure 2) suggest that, all other things being equal, the carrier mobilities should be comparable. However, the slightly smaller mobility of PDI-8CN$_2$ relative to PDI-8 may be due in part to the slight torsion of the PDI-8CN$_2$ core (Figure 12), resulting in weaker intermolecular interactions, consistent with the lower melting point of PDI-8CN$_2$ relative to PDI-8 (Figure S2). Additionally, the slight decomposition of PDI-8CN$_2$ during film deposition may introduce contaminant-derived traps in the film (Figure S2).

The DFT level electronic structure calculations performed here on NDI-8CN$_2$ suggest that dicyanation of the NDI core does not lead to the core torsion observed in the perylene case (Figure 14), most likely because the cyano functionality in the NDI case does not have a proximate hydrogen atom with which to interact. Thus it seems reasonable, given this lack of core distortion upon cyanation and the similar electron mobility relative to the uncyanated derivative, that the crystal packing in NDI-8 and NDI-8CN$_2$ is very similar.

Within the 1*H*,1*H*-perfluorobutyl series, the core-halogenated materials still exhibit substantially lower mobilities relative to the unsubstituted parent. This can be attributed in part to the crystal packing effects discussed above (Figure 13). However, the presence of more than one family of XRD diffraction peaks for these films suggests a less favorable microstructure vs the high mobility materials (Figure 3).

The AFM images also exhibit large surface features protruding from the PDI–FBr$_2$ film (Figure 5), similar to the *n*-octyl analogue that has similarly low carrier mobility (Figure 4). The PDI-FCl$_4$ surface morphology is unique compared to the other materials, which is consistent with this being the only material

(120) Dimitrakopoulos, C. D.; Brown, A. R.; Pomp, A. *J. Appl. Phys.* **1996**, *80*, 2501–2508.
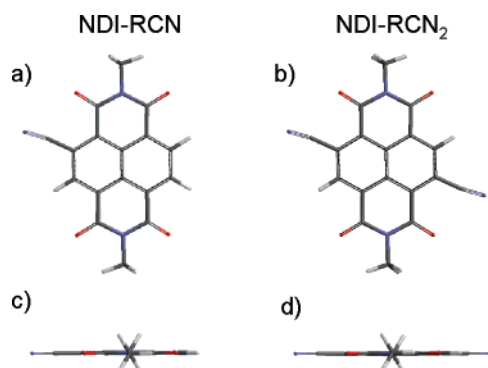
Figure 14. Calculated molecular geometries for *N*,*N*′-methyl derivatives NDI-RCN (a and c) and NDI-RCN$_2$ (b and d). The face-on views of (a) NDI-RCN and (b) NDI-RCN$_2$ show the distortion of the C(aromatic)−CN bond angle to ∼172°, while the view along the *N*−*N*′ axes in (c) and (d) reveal the rigorously planar aromatic core.

not exhibiting a first-order diffraction feature in the XRD having the molecular long axis dimension (Figure 3). Interestingly, in the R^F-substituted case, the dicyanated PDI-FCN$_2$ derivative exhibits much greater FET mobility than the unsubstituted PDI-F, in contrast to the *n*-octyl case which displays the opposite trend (Table 3). The XRD of PDI-F only exhibits a single family of diffraction peaks as in the high mobility *n*-octyl materials; however, the AFM shows large protrusions from the film, similar to the low mobility PDI-Br$_2$-based materials. PDI-FCN$_2$ exhibits an unusually large mobility for a material with multiple families of diffraction peaks; however the AFM evidences a much smoother and homogeneous film morphology. The high mobility of PDI-FCN$_2$ can likely be explained by a favorable orientation for charge transport as indicated by the ∼60° tilt angle from the XRD (Table 2), which is significantly more upright than the other semiconductors in this study.

Effects of Molecular Electron Affinity on OFET Performance in Vacuum. Given that the packing and film-forming properties of the semiconductors investigated in this study vary greatly, analysis of electron affinity effects on OFET response, although necessarily qualitative, provides useful guidelines for understanding electrical properties and ambient-stable n-channel materials. For OFETs characterized under vacuum, the observed effects on the present arylene diimide OFET response properties of electron affinity as expressed by solution-phase reduction potentials are primarily restricted to V_{th} and I_{on}/I_{off}, which generally decrease with increasing electron affinity for all of the present materials (Table 3 and Figure 9). For V_{th}, the decrease reflects the relative ease of creating mobile n-type carriers in the material, which correlates with mobile carrier creation at lower gate bias. Moreover, the depression in I_{on}/I_{off} with increasing electron affinity is a reflection of the larger source−drain current observed at $V_g = 0$ V indicating high I_{off} values. The greater carrier density at $V_g = 0$ V for the larger electron affinity semiconductors likely reflects greater susceptibility to charge carrier-generating impurities (doping).

Effects of Ambient Environment on OFET Performance. When operating the present OFETs in ambient atmosphere, the electrical properties of the air-unstable materials exhibit large device-to-device variations (Table 3), presumably also reflecting minor differences in film microstructure/morphology (Figures 2 and 4) and degrees of O$_2$ intrusion. Direct comparison of the electrical properties still indicates no obvious trend in mobility

values as a function of electron affinity (Figure 9). However, the relative degradation in OFET mobility measured in air relative to vacuum operation does generally parallel trends in electron affinity for the *n*-octyl materials (Table 3). The decrease in mobility by a factor of 1600× for PDI-8, 80× for PDI-8Cl$_4$, and 17× for NDI-8CN demonstrates the extreme sensitivity of these materials to ambient-based charge traps, as well as decreasing sensitivity with increasing electron affinity. The materials with highest electron affinity, PDI-8CN$_2$ and NDI-8CN$_2$, show far less degradation in carrier mobility measured in air vs vacuum. PDI-8CN$_2$ mobility degradation is minimal, and the factor of 1.4× OFET mobility decrease for NDI-8CN$_2$ is slight. For the air-unstable materials PDI-8, PDI-8Cl$_4$, and NDI-8CN, the decrease in OFET mobility is nearly instantaneous upon breaking vacuum; however, after 18 months of air exposure the air-stable devices fabricated with PDI-8CN$_2$ and NDI-8CN$_2$ exhibit electron mobilities ∼0.10 cm^2 V^{-1} s^{-1}. The long-term stability of materials with E_{red1} positive of −0.06 V vs SCE suggests that the charge carrier stability is largely responsible for the resistance of the electrons to trapping.

For ambient OFET operation, V_{th} is very large for all semiconductors with E_{red1} more positive than −0.06 V vs SCE (Figure 9 and Table 3). In ambient, the I_{on}/I_{off} ratios are roughly the same for PDI-8, PDI-8Cl$_4$, and PDI-8CN$_2$ OFETs; however the decrease in this ratio for PDI-8 and PDI-8Cl$_4$ relative to their vacuum performance is due to the lower I_{on} (Figures 7 and 8) which reflects the trapping tendencies of ambient species. Moreover, the molecular electron affinities of these molecules *do affect* the magnitudes of the change in their vacuum vs ambient response properties. The electron mobility of the lowest electron affinity material PDI-8 decreases by a factor of 1600× in air relative to vacuum, while PDI-8Cl$_4$ with a higher electron affinity decreases by a factor of 80×, and NDI-8CN with a still higher electron affinity only decreases by a factor of 17×. For the very high electron affinity materials PDI-8CN$_2$ and NDI-8CN$_2$, the decrease in electron mobility of devices operated in air is small or negligible relative to the standard deviation. Furthermore, the shift in V_{th} upon operation in ambient is ∼100 V for PDI-8 and NDI-8CN, ∼70 V for PDI-8Cl$_4$, and negligible for PDI-8CN$_2$ and NDI-8CN$_2$, the trend reflecting the decrease in trap state density for dicyanated derivatives (*vide infra*) and paralleling the trend in molecular electron affinity (Figure 9). This decrease in threshold voltage shift with increasing electron affinity suggests that the charge carriers become less susceptible to higher energy trap states. Interestingly, the average V_{th} shifts by ∼ −20 V for the most electron-deficient semiconductor, NDI-8CN$_2$, suggesting that doping is significant in this material. When comparing devices operated under ambient conditions, the electron carriers in semiconductors with lower LUMO energies (higher electron affinities) should be more stable and less affected by atmospheric species. This explains the general decrease in interfacial trap density with increasing *N*,*N*′-*n*-octyl PDI electron affinity as follows: PDI-8 (∼6 × 10^{13} cm^{-2}), PDI-8Cl$_4$ (∼4 × 10^{13} cm^{-2}), NDI-8CN (∼9 × 10^{13} cm^{-2}), PDI-8CN$_2$ (immeasurably low), and NDI-8CN$_2$ (immeasurably low). Thus, the negligible vacuum to ambient trap density increases for PDI-8CN$_2$ and NDI-8CN$_2$ films explain the ambient OFET stability. In contrast, the trap density increases dramatically (to >10^{13} cm^{-2}) for PDI-8Cl$_4$, NDI-8CN, and PDI-8 upon exposure of the films to ambient.

In comparison to the above results, all of the present $1H,1H$-perfluorobutyl-substituted semiconductor thin films afford air-stable OFETs (Table 3). The electron mobility degradation upon exposure of these materials to ambient atmosphere is minimal, similar to the cases of PDI-8CN$_2$ and NDI-8CN$_2$. However, PDI-F and PDI-FBr$_2$ have E_{red1} significantly negative of -0.06 V vs SCE (Table 1), which implies a fluorocarbon barrier mechanism discussed further below. Additionally, the fact that the XRD of the fluorocarbon materials exhibits multiple families of reflections (Figure 3) and the AFM shows substantially different film morphologies than those of the fluorine-free n-octyl analogues (Figures 4 and 5) suggests that the thin film morphology/microstructure in the $1H,1H$-perfluorobutyl derivatives changes significantly in comparison to that of the n-octyl materials, consistent with the model proposed by Katz et al. However in the case of PDI-F, the device cycling in ambient atmosphere demonstrates the kinetic sensitivity of I_d to degradation processes (Figure 10), which is also reflected in the substantial electron mobility decrease between cycles 0 and 1001. The sensitivity of PDI-F over repeated operation suggests that the crystal packing related barrier to atmospheric penetration (Figure 1) allows atmosphere-based charge trap inclusion over time/device operational stress, which leads to charge carrier trapping. The increase in trap density on repeated device cycling is further confirmed by the substantial positive shift in V_{th} over the course of the measurement. In contrast, the significant stabilization of electrons in the low LUMOs of PDI-8CN$_2$ relative to PDI-F leads to very stable device I_d and electron mobility despite the duration of atmospheric exposure/device operational stress, and the negligible electron trap density increase in these materials is reflected in the stable V_{th}. Further confirmation that the charge carrier stabilization in films of the high electron affinity dicyanated materials is responsible for the air-stability is found in the device cycling characteristics of PDI-FCN$_2$, which remain stable in I_d, carrier mobility, and V_{th} despite the use of the same $1H,1H$-perfluorobutyl substituents as PDI-F.

The V_{th} shifts and thus trap state density increases in these materials on going from vacuum to ambient OFET operation are statistically insignificant for all four N,N'-fluorocarbon substituted materials, despite having E_{red1} values more negative than those of air-unstable NDI-8CN and PDI-8Cl$_4$ (Table 3). I_{on}/I_{off} ratios for PDI-F and PDI-FCN$_2$ devices in air remain the same relative to the values in vacuum, consistent with a negligible increase in atmospheric-based traps. The slight decrease for PDI-FBr$_2$ and PDI-FCl$_4$ could reflect a slight increase in trap state density.

Analysis of Ambient Stability Mechanisms. The stability of PDI-8CN$_2$ and NDI-8CN$_2$ OFETs in ambient, compared with the other air-unstable materials investigated here, suggests that the origin of the OFET air stability is largely due to the energetic stabilization of electrons in the extremely low-lying LUMOs of the semiconductor. Since PDI-8CN$_2$ has slightly weaker intermolecular cohesive interactions than PDI-8, as evidenced by the slightly lower carrier mobility in a vacuum (Table 3) and the melting point (Table S2), and similar packing motif/film microstructure properties (Figures 13 and 2), the hypothesis that a crystal packing-based barrier is primarily responsible for the charge carrier air-stability seems unlikely in this case. Similarly, the case of air-stable NDI-8CN$_2$ devices, exhibiting

very similar film microstructure/morphology to air-unstable NDI-8CN devices (Figures 2 and 4), suggests that film characteristics are not responsible for the environmental stability of the NDI-8CN$_2$. In further support of the contention that the dicyanated semiconductors do not owe their air stability to a crystal packing barrier, the bulk of the cyclohexyl group at the N,N'-positions of the air-stable semiconductor PDI-CN$_2$ prevents close packing (Chart 1), which is consistent with the somewhat lower maximum mobility of 0.1 cm^2 V^{-1} s^{-1} for this material.[31]

Since the energetic stabilization of the electrons in the low lying LUMOs of PDI-8CN$_2$ and NDI-8CN$_2$ materials is likely the major contributing factor to the air stability of their OFETs, it follows that a reduction potential more positive that ~ -0.1 V vs SCE correlates with resistance to atmosphere-based electron traps in arylene diimide thin films (Figure 9). In comparison to the commonly studied materials discussed in the introduction (Charts 1 and 2), the electrochemical air-stability window defined by this study appears to pertain for other materials as well. Specifically, air-stable perhalogenated phthalocyanines F$_{16}$CuPc and Cl$_{16}$CuPc exhibit $E_{red1} \approx -0.1$ V vs SCE. In OFETs fabricated with thin films of arylene diimides NDI-8CN and PDI-8Cl$_4$ having reduction potentials slightly more negative than -0.1 V vs SCE, the electrons are clearly vulnerable to charge trapping by ambient-atmosphere-based species (Table 3, and Figures 8 and 9). Similarly, materials such as DCMT with slightly more negative E_{red1} values of ~ -0.2 V vs SCE exhibit ambient-sensitivity (Chart 2).

For $1H,1H$-perfluorobutyl substituted semiconductors, the reduction potential vs SCE of PDI-F (-0.33 V) and PDI-FBr$_2$ (-0.24 V) clearly places the LUMO/charge carrier energetics within the regime of air-unstable n-octyl derivatives (Table 1 and Figure 9). Thus, it appears that the fluorocarbon-based packing mechanism proposed by Katz et al. for naphthalene diimides[48,62,63,77] is operative in perylene diimides as well. The case of PDI-FCl$_4$ is borderline since the reduction potential lies at -0.13 V vs SCE, which corresponds to the region of the energetic window where the transition from air-unstable to air-stable in the n-octyl substituted materials is observed. The fluorinated material PDI-FCN$_2$ ($E_{red1} = +0.03$ vs SCE) probably derives its air stability from a combination of a fluorocarbon-based mechanism and orbital/carrier energetic stabilization.

If the model proposed earlier for n-type air stability is indeed operative,[42] based on the results of the n-octyl-substituted arylene diimides, the overpotential for charge carrier trapping by O$_2$ in ambient air for arylene diimide semiconductor films should be approximately 0.6 V. Additionally, the air stability of PDI-F, PDI-FBr$_2$, and PDI-FCl$_4$ OFETs strongly suggests that the previously proposed crystal-packing-based air-stability mechanism is related to the presence of fluorocarbon chains, as opposed to the minimal electron-withdrawing effects on the arylene imide semiconductors.

While it appears that energetic stabilization of the electron carriers plays a major role in the ambient OFET stability of the n-type PDI−CN$_2$ and NDI-8CN$_2$ semiconductors, the role of other factors which are not directly and quantitatively accessible with the present measurements cannot be discounted. The present evaluation of carrier energetics in these films is extrapolated from solution phase measurements on solvated single molecules. In solution, we previously showed that cyanated-PDI radical anions are stable in partially aerated

solutions; however, we also showed that deaeration enhances the long-term stability of the solvated radical anions.[64] This observation suggests that the thin film morphology/microstructure, in addition to the aforementioned film energetics, contributes to electron stabilization. Additionally, the large device-to-device variation in FET electrical parameters, μ and V_{th}, for the air-unstable devices could be indicative of subtle thin film microstructure/morphology/crystal packing effects that modulate atmospheric charge carrier trap penetration into the semiconductor thin films. Therefore, design criteria for air-stable n-channel OFET materials should account for both carrier energetics and solid-state/thin film packing and barrier properties.

Conclusions

The results of this study indicate that core substitution of arylene diimide semiconductors induces large variations in electron mobility due to geometric distortions of the arylene skeleton and consequent weakening of intermolecular $\pi-\pi$ overlap. Therefore, in order to achieve substantial OFET mobilities with core-functionalized arylene diimides, the substituents must be chosen to minimize such distortions and their effects on close molecular packing. Additionally, we also estimate for the first time that the overpotential to reaction of PDI and NDI n-type charge carriers with ambient O_2 in aryleneimide films is ~0.6 V, meaning that air-stable OFET materials should be accessible with properly designed arylene cores having the correct electron-withdrawing substituents.

Further studies on additional materials families should prove informative in determining how broadly this overpotential can be generalized to thin film organic electronic materials. Comparison of OFETs with semiconductor air-stability based on electron energetic stabilization vs a fluorocarbon-based crystal packing barrier leads us to conclude that semiconductors providing energetic carrier stabilization lead to long-term resistance to OFET electrical parameter degradation, while semiconductors owing air stability to ambient-based trap exclusion show significantly more OFET parameter erosion over air exposure duration/device stressing.

Supporting Information Available: Experimental details including synthesis, absorption/emission spectra, XRD of all films, AFM of all films, and logarithmic/square root transfer data. This material is available free of charge via the Internet at http://pubs.acs.org.

JA075242E